NEUTRINO INTERACTION ANALYSIS WITH AN AUTOMATIC SCANNING SYSTEM IN THE OPERA EXPERIMENT

A THESIS SUBMITTED TO
THE GRADUATE SCHOOL OF NATURAL AND APPLIED SCIENCES
OF
MIDDLE EAST TECHNICAL UNIVERSITY

BY

BEHZAD HOSSEINI

IN PARTIAL FULFILLMENT OF THE REQUIREMENTS
FOR
THE DEGREE OF MASTER OF SCIENCE
IN
PHYSICS

JUNE 2012

Approval of the thesis:

NEUTRINO INTERACTION ANALYSIS WITH AN AUTOMATIC SCANNING SYSTEM IN THE OPERA EXPERIMENT

submitted by **BEHZAD HOSSEINI** in partial fulfillment of the requirements for the degree of **Master of Science in Physics Department, Middle East Technical University** by,

Prof. Dr. Canan Özgen _____
Dean, Graduate School of **Natural and Applied Sciences**

Prof. Dr. Mehmet T. Zeyrek _____
Head of Department, **Physics**

Prof. Dr. Ali Murat Güler _____
Supervisor, **Physics Dept., METU**

Examining Committee Members:

Prof. Dr. Ramazan Sever
Physics Dept., METU _____

Prof. Dr. Ali Murat Güler
Physics Dept., METU _____

Prof. Dr. Osman Yılmaz
Physics Dept., METU _____

Prof. Dr. Ali Ulvi Yılmazer
Physics Engineering Dept., Ankara University _____

Assoc. Prof. Dr. İsmail Turan
Physics Dept., METU _____

Date: _____

I hereby declare that all information in this document has been obtained and presented in accordance with academic rules and ethical conduct. I also declare that, as required by these rules and conduct, I have fully cited and referenced all material and results that are not original to this work.

Name, Last Name: BEHZAD HOSSEINI

Signature :

ABSTRACT

NEUTRINO INTERACTION ANALYSIS WITH AN AUTOMATIC SCANNING SYSTEM IN THE OPERA EXPERIMENT

Hosseini, Behzad

M.Sc., Department of Physics

Supervisor : Prof. Dr. Ali Murat Güler

June 2012, 68 pages

The OPERA experiment was designed to search for $\nu_\mu \rightarrow \nu_\tau$ oscillations through the observation of ν_τ charged-current interactions in the OPERA target. This search requires a massive detector and very high spatial accuracy. Both requirements are fulfilled in the OPERA detector by using nuclear emulsion and lead plate in a modular structure called ECC brick. The OPERA detector consists of 150,000 ECC bricks and electronic detectors. The data taking was started in 2007 and is going on smootly. About 4000 neutrino interactions have been located so far. In this thesis, a detailed Data/MC comparisons of located neutrino events have been done, and analysis of neutrino events located using an automatic microscope system at METU is presented.

Keywords: Neutrino, Neutrino Oscillation, Nuclear Emulsion, Charm Particle

ÖZ

OPERA DENEYİNDE OTOMATİK TARAMA SİSTEMİYLE NÖTRİNO ETKİLEŞİM ANALİZİ

Hosseini, Behzad
Yüksek Lisans, Fizik Bölümü
Tez Yöneticisi : Prof. Dr. Ali Murat Güler

Haziran 2012, 68 sayfa

OPERA deneyi, hedefte ν_τ yüklü-akım etkileşmelerini gözlemleyerek $\nu_\mu \rightarrow \nu_\tau$ osilasyonlarını araştırmak için tasarlanmış bir deneydir. Böyle bir araştırma için, büyük kütleli ve yüksek posizyon hassasiyete sahip olan bir dedektöre ihtiyaç vardır. Bütün bu özellikler OPERA dedektöründe kullanılan emülsiyon filmleri ve kurşun plakaların oluşturduğu birimler ile sağlanmıştır. Dedektör bu özellikteki 150,000 tane birimden ve elektronik algılayıcıdan oluşmaktadır. Deneyde veri alımı 2007 yılında başlamış ve halen devam etmektedir. Bu zaman kadar 4000 nötrino etkileşmesi kaydedilmiştir. Hazırlanan bu tezde, belirlenmiş nötrino etkileşimleri için Data/MC karşılaştırmaları detaylı bir şekilde yapılmış, analizleri ise ODTU Fizik Bölümü'nde bulunan otomatik tarama mikroskobu ile gerçekleştirilmiştir.

Anahtar Kelimeler: Nötrino, Nötrino Salınımları, Nükleer Emülsiyon, Charm Parçacığı

To my family

ACKNOWLEDGMENTS

The work presented in this thesis would not have been possible without the involvement of a number of people. I would like to thank the following persons in particular:

First of all, I would like to thank to my supervisor Prof. Dr. Ali Murat Güler for giving me an opportunity to involve in the OPERA Collaboration, and his guidance, motivation, understanding, and patience, added considerably to my graduate experience.

I would like to thank to Mustafa Kamıscıoglu and Serhan Tufanlı for their help on this work, without their precious efforts completing this study would be impossible.

Another thanks goes to my group members Kemal Oktay Balıkçı, Çağın Güneş, Navid Hosseini, Ali Murat Sözen and specially Deniz Bender and Özgür Altınok for their friendship and for their helps.

A special thanks goes to Fahimeh Qasemnezhad for her help during writing this thesis.

I would like to thank to all the LNGS people that we worked together in Gran Sasso.

I would like to thank to INFN for the financial support during my stays in LNGS, also to TUBITAK (The Scientific and Technological Research Council of Turkey) for 25 months financial support in this study.

Of course a big thanks goes to my parents, my sister and her husband for their endless support and also to my sweety niece Jino for her kind wishes.

Finally thanks to all of my friends for their endless supports and believe in me.

TABLE OF CONTENTS

LIST OF TABLES

TABLES

LIST OF FIGURES

FIGURES

CHAPTER 1

INTRODUCTION

The history of neutrinos dates back to the early 1930′s. Before the discovery of the neutron, it was believed that the nucleus is composed of protons and electrons. Therefore, in this framework, the β-decay would be similar to the alpha decay. However, the study of beta radioactivity posed a serious problem: the emitted electrons do not have a single energy rather their spectrum is continuous. That is, energy and momentum were not conserved. In 1930, Wolfgang Pauli, proposed a solution for the missing energy in the β-decay. His solution was to introduce a third particle which was neutral, had a small mass, and had spin 1/2 [1]. In his words, this was a "desperate remedy" [2] for the problem at stake and by doing this, he was able to save the energy and angular momentum conservation laws. Although no one paid any attention to his proposal in the beginning, it was 1933 when Enrico Fermi, introduced Pauli′s particle as "neutrino" for the first time. In the same year, Fermi wrote down the necessary theoretical work and described the interactions of the neutrino with other elementary particles in this theory [3]. After Fermi′s theory, neutrinos became one of the most intriguing research areas of elementary particle physics.

Although Pauli and Fermi worked on neutrinos and introduced them, there was a great suspicion about the existence of neutrinos for many years. For example, Niels Bohr was not persuaded about the existence of these particles. In addition, Sir Arthur Eddington, remarked that "in an ordinary way I might say that I do not believe in neutrinos... Dare I say that experimental physicists will not have sufficient ingenuity to make neutrinos?" [2]. However, about twenty years later, Fred Reines and Clyde Cowan proved Pauli′s "desperate remedy." In 1951, Reines and Cowan decided to work on detecting the neutrino near a nuclear reactor, realizing that nuclear reactors could provide a neutrino flux of 10^{13} neutrinos per square centimeter per second. They also recognized that recently developed organic scintillating liquids

would allow them to build the massive detector they required. They first installed the detector in Hanford nuclear reactor. But the background signals, due to cosmic rays, were very high at that place. In 1955, they relocated the detector in the Savannah River nuclear reactor. The place of the detector was only 11 meters away from the reactor center and 12 meters deep in underground [4]. That year they were able to observe neutrinos, and finally in 1956 they reported to Pauli with a telegram reading: "We are happy to inform you that we have definitely detected neutrinos from fission fragments by observing inverse β-decay of protons." Pauli's reply to this was, "Thanks for the message. Everything comes to him who knows how to wait" [2]. With that discovery the long way of research on neutrinos has begun and in 1995 Reines was awarded with the Nobel Prize.

The type of neutrino discovered by Reines and Cowan was called as electron neutrino later [5, 6]. In 1962, experiments at Brookhaven National Laboratory showed that a second type of neutrino related with muons exists and behaves slightly differently from the electron neutrinos [7]. This type of neutrino is called "muon neutrino" since it emerges with muon. The existence of the third type of neutrino was inferred when the tau lepton, was discovered by Martin Perl at SLAC (Stanford Linear Accelerator Center) in 1975 [8]. In later years the DONUT (Direct Observation of the Nu Tau) experiment [9] which was a Fermilab experiment announced the first direct observation of tau neutrino interactions.

Since neutrinos are neutral leptons, they interact with matter through only weak force. Given the small cross section of weak interaction, the observation of neutrinos is very difficult. It requires massive detector and dense neutrino beam. The other distinct feature of the neutrino is its mass. In the Standard Model of particle physics [10], neutrinos are defined as massless, neutral leptons. Therefore, physics of massive neutrino is beyond the Standard Model. There are several experimental studies to measure the neutrino mass directly. However, their sensitivity is not sufficient to measure absolute masses so far. Therefore they can only put a limit on the neutrino masses. The present best limits on the neutrino masses are:

$$m_{\nu_e} < 2.2 \quad eV \qquad [11], \tag{1.1}$$

$$m_{\nu_\mu} < 170 \quad keV \qquad [12], \tag{1.2}$$

$$m_{\nu_\tau} < 15.5 \quad MeV \quad [13]. \tag{1.3}$$

On the other hand neutrino oscillation experiments can measure mass-square differences of the neutrinos. But these experiments are not sensitive to the absolute values of neutrino masses.

There are several sources of neutrinos. Some of them are artificial like nuclear reactors and particle accelerators. In addition to artificial sources, there are also natural sources of neutrinos like solar and Atmospheric neutrinos. According to the solar theories, the sun emits 65×10^9 (65 billion) neutrinos that pass through every square centimeter of the earth in every second [14]. Neutrinos are also produced in the atmosphere through the interaction of the high-energy protons with the nuclei of the atmosphere. These reactions largely result in the creation of the charged and neutral π-mesons, which decay into neutrinos:

$$\pi^{\pm} \longrightarrow \mu^{\pm} + \nu_{\mu}(\bar{\nu_{\mu}}); \tag{1.4}$$

$$\mu^{\pm} \longrightarrow e^{\pm} + \nu_{\mu}(\bar{\nu_{\mu}}) + \nu_{e}(\bar{\nu_{e}}). \tag{1.5}$$

It is clear that the flux of cosmic rays, that are responsible for Atmospheric neutrino production at low energy are the same throughout the Earth. In addition to solar and Atmospheric neutrinos, there are geoneutrinos which are produced by beta decay of radioactive elements in the Earth′s natural radioactivity.

The thesis is organized as follows: in the next chapter, a theoretical overview on neutrino oscillation will be given. In Chapter 3, the OPERA experiment will be explained in details and physics performances will be represented. In Chapter 4, the Emulsion Scanning System used in OPERA experiment will be described in detail and the OPERA events which have been analyzed with Emulsion Scanning System at METU will be presented. In Chapter 5, Data/MC comparisons of ν_{μ} Charged-Current (CC) events and ν_{μ}CC-Charm events, located so far in the OPERA experiment, are given.

CHAPTER 2

NEUTRINO OSCILLATIONS

The beginning of the twenty-first century was the time of sensational discoveries in the field of neutrino physics. The results, obtained up to the present time, trigger further experimental and theoretical studies to evolve the properties of neutrinos. One of the interesting properties of neutrino is the neutrino oscillation which was proposed by Bruno Pontecorvo in 1956.

Neutrinos oscillations are the consequence of flavor mixing. In the following, the quantum mechanical formulation of neutrino oscillations are described.

Let's first consider the neutrino oscillations for the two flavor case, i.e. electron and muon.

The wave functions of electron and muon neutrinos as a function of time are subject to the Schrodinger equation:

$$i\frac{\partial \Psi}{\partial t} = \hat{H}\Psi \;\; ; \;\; \Psi(t) = \begin{pmatrix} \nu_e(t) \\ \nu_\mu(t) \end{pmatrix} \tag{2.1}$$

$$i\frac{\partial}{\partial t}\begin{pmatrix} \nu_e(t) \\ \nu_\mu(t) \end{pmatrix} = \begin{pmatrix} E_e & H_{int} \\ H_{int} & E_\mu \end{pmatrix}\begin{pmatrix} \nu_e(t) \\ \nu_\mu(t) \end{pmatrix} \tag{2.2}$$

where,

$$\nu_k(t) \equiv |\nu_k(t)\rangle \;\; ; \;\; k = e \;\; , \;\; \mu. \tag{2.3}$$

$$I_{\nu_k}(t) = \langle \nu_k(t)|\nu_k(t)\rangle \tag{2.4}$$

Introducing the wave functions of the $\nu_1(t)$ and $\nu_2(t)$, mass eigenstates, for which the matrix of the Hamiltonian operator in Equation 2.2 is diagonal, are the following:

$$i\frac{\partial}{\partial t}\begin{pmatrix} \nu_1(t) \\ \nu_2(t) \end{pmatrix} = \begin{pmatrix} E_1 & 0 \\ 0 & E_2 \end{pmatrix}\begin{pmatrix} \nu_1(t) \\ \nu_2(t) \end{pmatrix}. \tag{2.5}$$

The transition from the mass eigenstates $\nu_1(t)$, $\nu_2(t)$ to neutrino eigenstates $\nu_e(t)$, $\nu_\mu(t)$ and back again is possible through a unitary matrix, where the angle θ is called "mixing angle".

$$\begin{pmatrix} \nu_e(t) \\ \nu_\mu(t) \end{pmatrix} = \begin{pmatrix} \cos\theta & -\sin\theta \\ \sin\theta & \cos\theta \end{pmatrix}\begin{pmatrix} \nu_1(t) \\ \nu_2(t) \end{pmatrix}; \tag{2.6}$$

$$\nu_e(t) = \nu_1(t)\cos\theta - \nu_2(t)\sin\theta; \tag{2.7}$$

$$\nu_\mu(t) = \nu_2(t)\cos\theta + \nu_1(t)\sin\theta; \tag{2.8}$$

$$\begin{pmatrix} \nu_1(t) \\ \nu_2(t) \end{pmatrix} = \begin{pmatrix} \cos\theta & \sin\theta \\ -\sin\theta & \cos\theta \end{pmatrix}\begin{pmatrix} \nu_e(t) \\ \nu_\mu(t) \end{pmatrix}. \tag{2.9}$$

If there is no mixing ($\theta = 0$), the ν_1 and ν_2 coincide with $\nu_e(t)$ and $\nu_\mu(t)$. Therefore, oscillation is not possible.

Consider the case in which neutrino beam consists of only electron neutrino, that is $\nu_\mu(t) = 0$; $\nu_e(t) = 1$. Then Equations (2.7) and (2.8) become the $\nu_1(0) = \cos\theta$, and $\nu_2(0) = -\sin\theta$.

The time dependent wave function $\nu_e(t)$ can be obtained using Equation (2.5):

$$i\frac{\partial}{\partial t}\nu_1(t) = E_1\nu_1(t); \tag{2.10}$$

$$i\frac{\partial}{\partial t}\nu_2(t) = E_2\nu_2(t); \tag{2.11}$$

$$\nu_1(t) = \nu_1(0)exp(-iE_1t); \tag{2.12}$$

$$\nu_2(t) = \nu_2(0)exp(-iE_2t); \tag{2.13}$$

$$\nu_e(t) = \cos^2\theta exp(-iE_1t) + \sin^2\theta exp(-iE_2t). \tag{2.14}$$

The probability of observing electron neutrino at any time t, is given as

$$\begin{aligned} Prob(\nu_e \to \nu_e) = |\langle\nu_e(t)|\nu_e(t)\rangle| &= [\cos^2\theta exp(+iE_1t) + \sin^2\theta exp(+iE_2t)] \\ &\times[\cos^2\theta exp(-iE_1t) + \sin^2\theta exp(-iE_2t)] \\ &= \cos^4\theta + \sin^4\theta + \sin^2\theta\cos^2\theta[exp(+i(E_2 - E_1)t) + exp(-i(E_2 - E_1)t)]. \end{aligned} \tag{2.15}$$

By using following trigonometric identities

$$2\sin\theta\cos\theta = \sin 2\theta \;\; ; \;\; exp(i\alpha) + exp(-i\alpha) = 2\cos\alpha \;\; ; \;\; \cos\alpha = 1 - 2\sin^2\frac{\alpha}{2}. \tag{2.16}$$

Equation (2.15) can be rewritten as

$$\begin{aligned} Prob(\nu_e \rightarrow \nu_e) &= \cos^4\theta + \sin^4\theta + \sin^2\theta\cos^2\theta[exp(+i(E_2 - E_1)t) + exp(-i(E_2 - E_1)t)] \\ &= \cos^4\theta + \sin^4\theta + \sin^2\theta\cos^2\theta[2 - 4\sin^2\tfrac{(E_2-E_1)t}{2}] \\ &= \cos^4\theta + \sin^4\theta + 2\sin^2\theta\cos^2\theta - 4\sin^2\theta\cos^2\theta[\sin^2\tfrac{(E_2-E_1)t}{2}] \\ &= (\cos^2\theta + \sin^2\theta)^2 - 4\sin^2\theta\cos^2\theta[\sin^2\tfrac{(E_2-E_1)t}{2}] \\ &= 1 - \sin^2 2\theta\sin^2\tfrac{(E_2-E_1)t}{2}. \end{aligned} \tag{2.17}$$

The probability of detecting muon neutrinos in a beam which initially consists of only electron neutrinos,

$$Prob(\nu_e \rightarrow \nu_\mu) = 1 - Prob(\nu_e \rightarrow \nu_e) = \sin^2 2\theta\sin^2\frac{(E_2 - E_1)t}{2}. \tag{2.18}$$

It is more convenient to express the oscillation probability in terms of neutrino mass-square difference (Δm^2), and traveled distance (L). For this, consider the ultra-relativistic neutrinos; p $\gg$ m,

$$E = (p^2 + m^2)^{1/2} = p(1 + \frac{m^2}{p^2})^{1/2} = p + \frac{m^2}{2p}. \tag{2.19}$$

The Equation 2.18 can be rewritten as

$$\sin^2 2\theta\sin^2\frac{(E_2 - E_1)t}{2} = \sin^2 2\theta\sin^2\frac{\Delta m^2.L}{4E_\nu}. \tag{2.20}$$

Where neutrino energy (E_ν) is in GeV, neutrino mass-square difference (Δm^2) is in $(eV)^2$, and traveled distance (L) is in km.

Thus, if the mass square difference between neutrinos is small, one needs a long base-line L in order to observe the neutrino oscillations. After all simplifications, the oscillation probability for two flavor case is given as

$$P(\nu_\alpha \rightarrow \nu_{\alpha'}; L) = \sin^2(2\theta)\sin^2[1.27\Delta m^2(eV^2)\frac{L(km)}{E(GeV)}], \tag{2.21}$$

In the case of three neutrino flavors, the mixing matrix so called "PMNS" [15] is parameterized as

$$U = \begin{pmatrix} c_{12}c_{23} & s_{12}c_{13} & s_{12}e^{-i\delta} \\ -s_{12}c_{23} - c_{12}s_{23}s_{13}e^{-i\delta} & c_{12}c_{23} - s_{12}s_{23}s_{13}e^{-i\delta} & s_{23}c_{13} \\ s_{12}c_{23} - c_{12}s_{23}s_{13}e^{-i\delta} & -c_{12}s_{23} - s_{12}c_{23}s_{13}e^{-i\delta} & c_{23}c_{13} \end{pmatrix}, \tag{2.22}$$

where $c_{ij} = \cos\theta_{ij}$ and $s_{ij} = \sin\theta_{ij}$ in this formula; therefore, the mixing matrix contains three mixing angles (θ_{12}, θ_{13}, θ_{23}) and a phase angle δ which is responsible for the CP violation in the leptonic sector and oscillation probability $P(\nu_\alpha \rightarrow \nu_\beta)$ is given:

$$Prob(\nu_\alpha \rightarrow \nu_\beta; L) = |\langle\nu_\beta|\nu_\alpha\rangle|^2 = \delta_{\alpha\beta} - 4\Sigma U_{\alpha i}U^*_{\beta i}U^*_{\alpha j}U_{\beta j}sin^2(\frac{1.27\Delta m^2_{ij}L}{E}) \quad [16]. \tag{2.23}$$

2.1 Experimental Studies of Neutrino Oscillations

Neutrino oscillations can be traced back to the solar neutrino problem. After the discovery of electron neutrinos, the β-decay was understood, but this led soon to another problem. According to the solar models, the main mechanism for nuclear fusion in the sun is the "proton-proton chain." In this chain there are five reactions that produce neutrinos as shown in Figure 2.1.

2.1.1 Homestake: first evidence of solar neutrino deficit

In order to measure neutrino flux from sun, Raymond Davis, installed a radiochemical detector in the former Homestake gold mine in South Dakota. The detector consists of a tank containing 390 m^3 of perchlorethylene (C_2Cl_4).

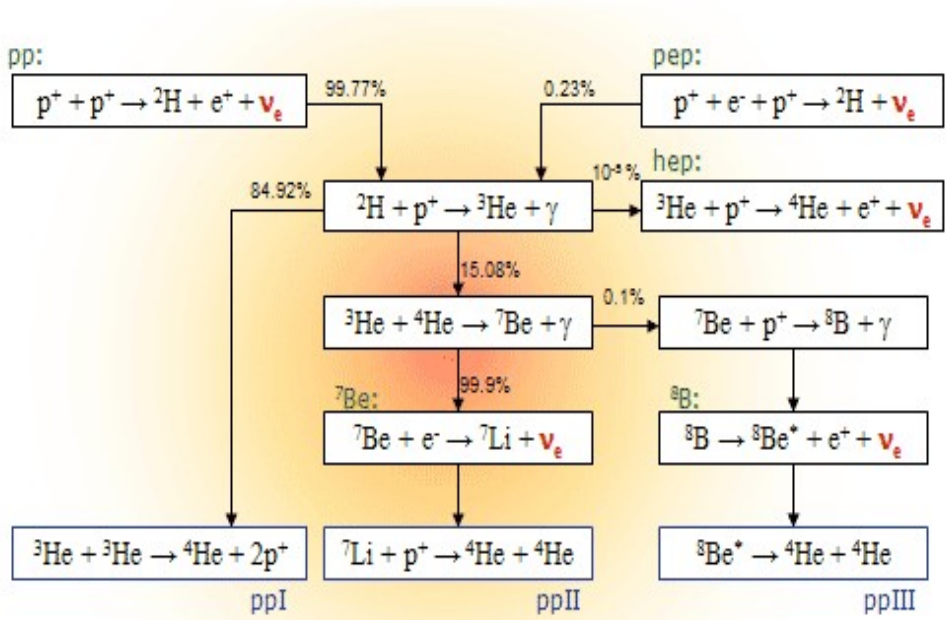

Figure 2.1: Proton-proton cycle [17].

The detection principle is based on the inverse β-decay. That is a stable ^{37}Cl isotope is transformed into a radioactive isotope of ^{37}Ar.

$$\nu_e + {}^{37}Cl \rightarrow {}^{37}Ar + e^-. \tag{2.24}$$

Finally, more than twenty years of data acquisition, the measured flux is much smaller then Standard Solar Model (SSM) [18] prediction, namely 1/3 of predicted amount,

$$\frac{\Phi_{Cl}^{Data}}{\Phi_{Cl}^{SSM}} = 0.33 \pm 0.03. \tag{2.25}$$

Therefore in the Homestake experiment indicates the possibility of the disappearance of solar neutrinos [19].

2.1.2 GALLEX-GNO, SAGE: evidence from the second set of solar neutrino deficit

The Homestake experiment has an energy threshold high enough to prevent the detection of neutrinos from the pp-cycle. Vadim Kuzmin introduced the possibility of using gallium for

detection in 1960, but the technique would have been developed thirty years later in the experiments GALLEX [20] and SAGE [21]. The applied technique for solar neutrino detection in these experiments is similar to one used in the Homestake experiment.

Solar neutrinos are detected through inverse β-decay:

$$\nu_e + {}^{71}Ga \rightarrow {}^{71}Ge + e^{-}. \tag{2.26}$$

In these experiments the number of neutrino interaction is estimated by counting ^{71}Ge atoms. This reaction has a threshold of 0.233 MeV, which allows the detection of all neutrinos in the proton-proton chain. These two experiments had different technologies. SAGE used a tank filled with pure liquid gallium while GALLEX-GNO used an aqueous solution containing gallium chloride ($GaCl_3$) and hydrochloric acid (HCl) [22].

The combined analysis of GALLEX, SAGE, and GNO data, gives

$$\frac{\Phi^{Data}}{\Phi^{SSM}} = 0.54 \pm 0.04 \tag{2.27}$$

Therefore, these experiments confirm the solar neutrino deficit.

2.1.3 Kamiokande and SuperKamiokande: evidence of the third set of solar neutrino deficit

Kamiokande and Super Kamiokande are parts of the family of detectors based on measuring the Cerenkov radiation emitted by the charged particles. These experiments are different then radiochemical experiments. Therefore, it provides an independent check for the solar neutrino deficit.

Kamiokande, the first water-Cherenkov detector, was 3 ktons of pure water. This detector was placed 1000 m underground in Kamioke mine in Japan. The construction of the detector was completed in 1984 and then took the data until 1995.

In 1996, the Kamiokande detector was upgraded to 50 kton of ultra pure water and became Super-Kamiokande. This detector, a huge cylindrical tank of 41.4 meters tall and 39.3 meters

in diameter, was filled with more than 50 ktons of ultra pure water. The detector is equipped 11,146 photomultipliers are oriented inwards to observe interactions, and 1,886 others are oriented outwards to detect particles coming from outside [23] (see Figure 2.2).

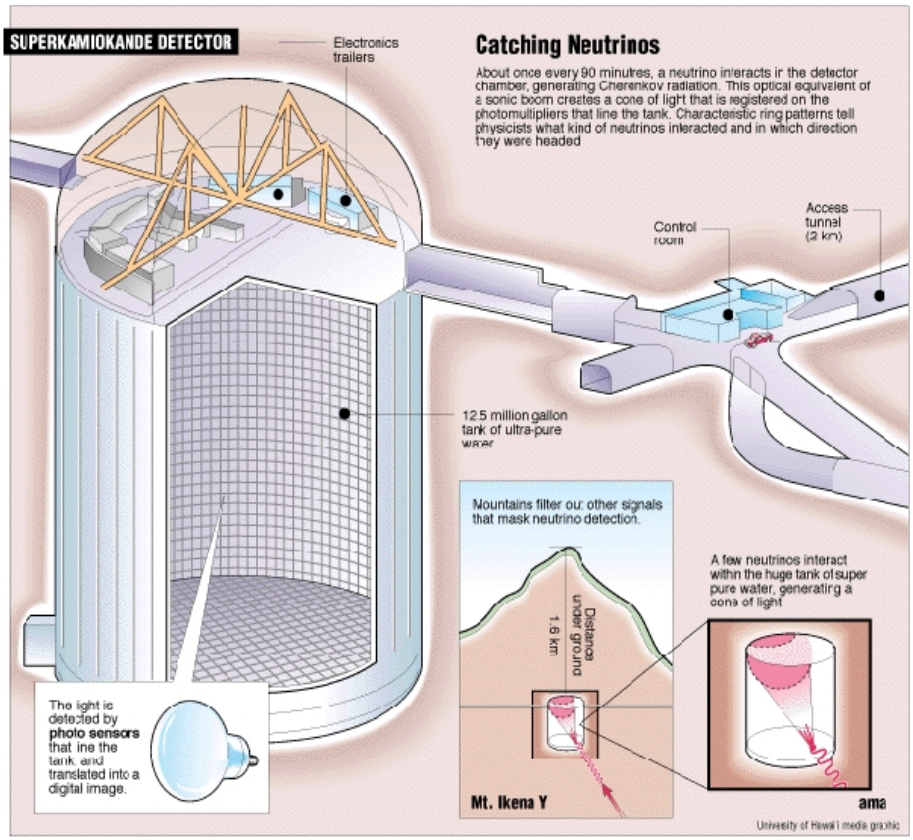

Figure 2.2: Super-Kamiokande detector.

In the Super-Kamiokande detector, neutrinos are detected through their elastic scattering with electrons:

$$\nu_x + e^- \rightarrow \nu_x + e^-, \tag{2.28}$$

where x = e, μ, and τ.

The measurement of Super-Kamiokande confirms the solar neutrino deficit. The ratio of measured solar flux to the predicted one is

$$\frac{\Phi_{SK}^{Data}}{\Phi_{SK}^{SSM}} = 0.465 \pm 0.015. \tag{2.29}$$

By using the different techniques and methods solar neutrino deficit has been confirmed. Table 2.1 shows the summary of solar neutrino measurements.

Table 2.1: Summary of all observation.

Experiment	Reactions	Threshold (MeV)	Results ($\frac{\Phi^{Data}}{\Phi^{SSM}}$)
Homestake	$\nu_e + {}^{37}Cl \rightarrow {}^{37}Ar + e$	0.814	0.33 ± 0.03
GALLEX-GNO, SAGE	$\nu_e + {}^{71}Ga \rightarrow {}^{71}Ge + e$	0.233	0.54 ± 0.04
Super-Kamiokande	$\nu_e + e \rightarrow \nu_e + e$	5.5	0.465 ± 0.015

Although Super-Kamiokande has had an important role in the study of the solar neutrino problem, this detector resulted in the major findings in the Atmospheric neutrinos.

In the Super-Kamiokande detector, neutrino interactions could be identified and classified by the Cerenkov radiation. Once identified, the events are classified, according to their topology. These events are further divided into three categories: fully contained (FC), partially contained (PC) or produced by an upward-going muon (UPμ) as shown in Figure 2.3. Then, the fully contained events in the detector are divided into two categories according to their energy: "sub-GeV" (E < 1.33 GeV) and "multi-GeV" (E > 1.33 GeV). In the end, a final classification is made according to the direction of the detected particle. This last characteristic gives the distance traveled by the neutrino before the interaction in the detector.

Since the production of Atmospheric neutrinos are isotropic, the number of downward-going neutrinos must be equal to the number of upward-going. Therefore, if there is no any effect like oscillation, one expects

$$N_l(\cos\theta_z) = N_l(-\cos\theta_z). \tag{2.30}$$

Where θ_z is zenith angle and shown in Fiqure 2.4.

Super-Kamiokande, measured the flux of ν_μ and ν_e as a function of zenith angle θ in 1998. Super-Kamiokande has observed a deficit of muon events for neutrinos crossing the Earth in the area $\cos\theta < 0$, (the neutrinos that have traveled a greater distance) than those with $\cos\theta > 0$. This phenomenon can be seen in Figure 2.5 and it is called "the atmospheric neutrino anomaly,". The deficit can be explained consistently by $\nu_\mu \rightarrow \nu_\tau$ oscillations.

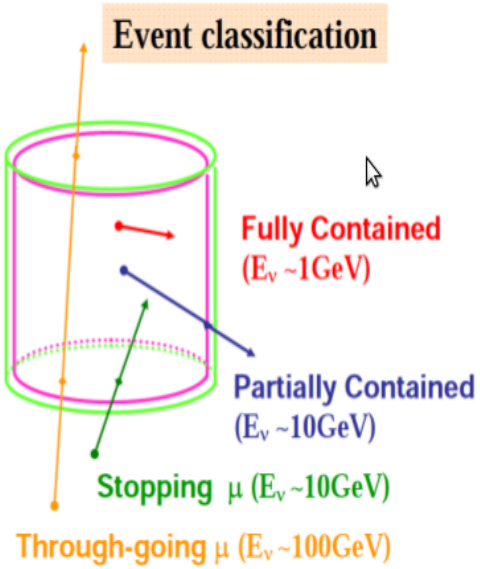

Figure 2.3: Classification of events in Super-Kamiokande detector.

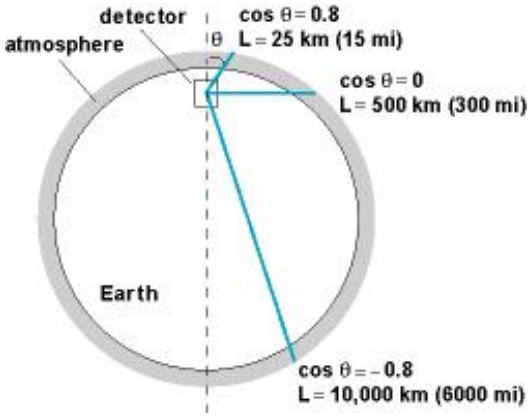

Figure 2.4: A view of cosmic rays arriving on the Super-Kamiokande detector.

The best fit value of oscillation parameters are $1.5\times10^{-3} < \Delta m^2_{23} < 3.4\times10^{-3}$, and $sin^2 2\theta_{23} > 0.92$ [24].

2.1.4 Sudbury Neutrino Observatory (SNO)

SNO-cherenkov detector was located in the Creighton Mine (Canada) at the depth of 2070 m. The detector is acrylic vessel with a diameter of 12 meters. It is filled with 1000 tons of ultra-

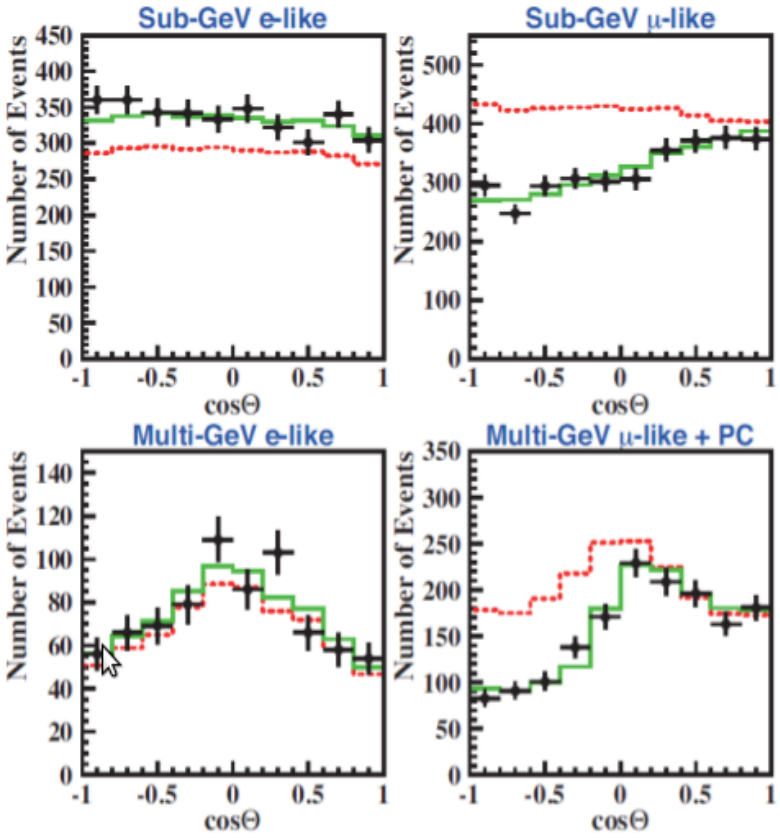

Figure 2.5: Zenith angle distributions for electron and muon events with visible energy < 1.33 GeV (sub-GeV) and > 1.33 GeV (multi-GeV). The dotted histograms show the non-oscillated Monte Carlo events, and the solid histograms show the expectations for $\nu_\mu \rightarrow \nu_\tau$ oscillations [25].

pure heavy water (D_2O). The Cherenkov radiation is registered by 9600 photo-multipliers, mounted on a sphere with a diameter of 17 meters surrounding the vessel. The detector is immersed in ultra-pure ordinary water, which is in the barrel cavity with a diameter of 22 meters and a height of 34 meters, excavated in the rock [26].

In Sudbury the "Sun boron" neutrinos

$$^8B \longrightarrow ^8 Be^* + e^+ + \nu_e, \tag{2.31}$$

were detected through the following reactions:

$$\nu_e + d \longrightarrow e^- + p + p, \qquad (CC) \tag{2.32}$$

$$\nu_x + d \longrightarrow \nu_x + n + p, \qquad (NC) \tag{2.33}$$

$$\nu_x + e \longrightarrow \nu_x + e. \qquad (ES) \tag{2.34}$$

The first reaction, Charged Currents (CC), is sensitive only to electron neutrinos (ν_e). The second one, Neutral Currents (NC), is sensitive to all neutrinos (x: e, μ, τ). In addition, the Elastic Scattering (ES) is sensitive to all flavors of neutrinos, but smaller for muon and tau neutrinos.

After 2-years of data taking, SNO collaboration measured the neutrino fluxes

$$\Phi_{SNO}^{CC} = 1.76^{+0.06}_{-0.05}(stat.)^{+0.09}_{-0.09}(syst.) \times 10^6 cm^{-2} s^{-1}, \tag{2.35}$$

$$\Phi_{SNO}^{ES} = 2.39^{+0.24}_{-0.23}(stat.)^{+0.12}_{-0.12}(syst.) \times 10^6 cm^{-2} s^{-1}, \tag{2.36}$$

$$\Phi_{SNO}^{NC} = 5.09^{+0.44}_{-0.43}(stat.)^{+0.46}_{-0.43}(syst.) \times 10^6 cm^{-2} s^{-1}. \tag{2.37}$$

Thus, if neutrinos can change from one flavor to another, the neutrino flux as measured by reaction (CC) Φ^{CC} (ν_e) must be less than the flux measured by the reaction of (ES) Φ^{ES} (ν_x).

In the first series of measurements, which was carried out using the CC interactions, there was a deficit in the electron neutrino flux. The SNO data, provides an estimate of solar neutrino flux through the reaction in Equation (2.31). The measured flux is in good agreement with the SSM predictions.

The best fit value of Δm^2_{12} and solar mixing angle $sin^2(\theta_{12})$ are

$$\Delta m^2_{12} = 7.1^{+0.5}_{-0.5} \times 10^{-5}\ eV^2, \tag{2.38}$$

and

$$sin^2(\theta_{12}) = 0.30^{+0.09}_{-0.04}\ ,\ \ \theta_{12} = 32.5^o. \tag{2.39}$$

2.1.5 K2K Experiment

After the first results of the Super-Kamiokande experiment, a confirmation of the oscillation was necessary. The best way to do this is to use a controlled neutrino beam. That is an accelerator experiment. Soon after Super-Kamiokande measurement, K2K experiment at Japan was proposed to confirm the Super-Kamiokande results.

A muon neutrino beam produced at KEK and sent to Super-Kamiokande detector located in Kamioka, 250 km away. The average energy of the muon neutrino beam is 1.3 GeV. Therefore, by comparing the measured flux for Super-Kamiokande and KEK, they measured the ν_μ disappearance.

Their results are consistent with Super-Kamiokande measurements. The mass-squre difference Δm^2_{23} and mixing angle $sin^2(\theta_{23})$ are [27]

$$sin^2 2\theta_{23} = 1, \tag{2.40}$$

and

$$1.8 \times 10^{-3} eV^2 \ < \ \Delta m^2_{23} \ < \ 3.6 \times 10^{-3} eV^2. \tag{2.41}$$

2.1.6 MINOS Experiment

After Super-Kamiokande result, two long-base experiments: one in USA and the other in Europe were proposed to search for the neutrino oscillations in the parameter space defined by the Super-Kamiokande experiment. The MINOS experiment uses two detectors. One is located near to the beam and the other is at a distance of 725 km from Fermilab (USA)[28]. By comparing neutrino flux measured at near and far detectors, MINOS confirmed neutrino oscillations in the disappearance mode.

The best fit values of oscillation parameters are [29]

$$sin^2 2\theta_{23} = 1, \tag{2.42}$$

and

$$\Delta m^2_{23} = 2.74 \times 10^{-3} eV^2. \tag{2.43}$$

All experimental observations so far on neutrino oscillations has been done in the disappearance mode which measures a deficit in the expected neutrino flux. On the other hand, the appearance experiments which measure the appearance of a new neutrino flavor, gives a solid proof of the oscillations. Therefore the OPERA experiment was designed to search for ν_τ appearance in an almost pure ν_μ beam.

In next chapter the OPERA detector and $\nu_\mu \rightarrow \nu_\tau$ oscillation search will be discussed.

CHAPTER 3

THE OPERA EXPERIMENT

OPERA (**O***scillation* **P***ro ject with* **E***mulsion t***R***acking* **A***pparatus*) is a long baseline experiment designed to provide conclusive result for $\nu_\mu \rightarrow \nu_\tau$ oscillations in the parameter space indicated by the Super-Kamiokande experiment [30].

The OPERA detector is located in Gran Sasso underground laboratory, 732 km away from CERN where CNGS (CERN Neutrino to Gran Sasso) neutrino beam is produced [31, 32]. A search for $\nu_\mu \rightarrow \nu_\tau$ oscillations in appearance mode requires a detector of large mass and high spatial resolution. Both requirements are fulfilled by using ECC (Emulsion Cloud Chamber) technology in the experiment. It consists of a sequence of 56 lead plates and 57 emulsion plates forming a sandwich structure. The emulsions are used as tracking detectors with a submicron spatial resolution. While the lead plates constitutes the large detector mass. Each ECC brick has a transverse dimension of $10 \times 12.5\ cm^2$ and a thickness of 7.54 cm for a total weight of 8.3 kg [33, 34].

3.1 The CNGS Neutrino Beam

The CNGS (Cern Neutrino to Gran Sasso) is a wide-band neutrino beam which is produced at CERN and directed towards the INFN Gran Sasso underground laboratory. The neutrino beam travels 732 km before reaching to the OPERA detector.

The production of neutrino beam requires several steps in the accelerator complex at CERN. First, protons are accelerated in SPS at the energy of 400 GeV. Then the extracted protons are transported through the transfer line to the CNGS target, and secondary pions and kaons are produced. These pions and kaons are guided with two focusing lenses, named horn and

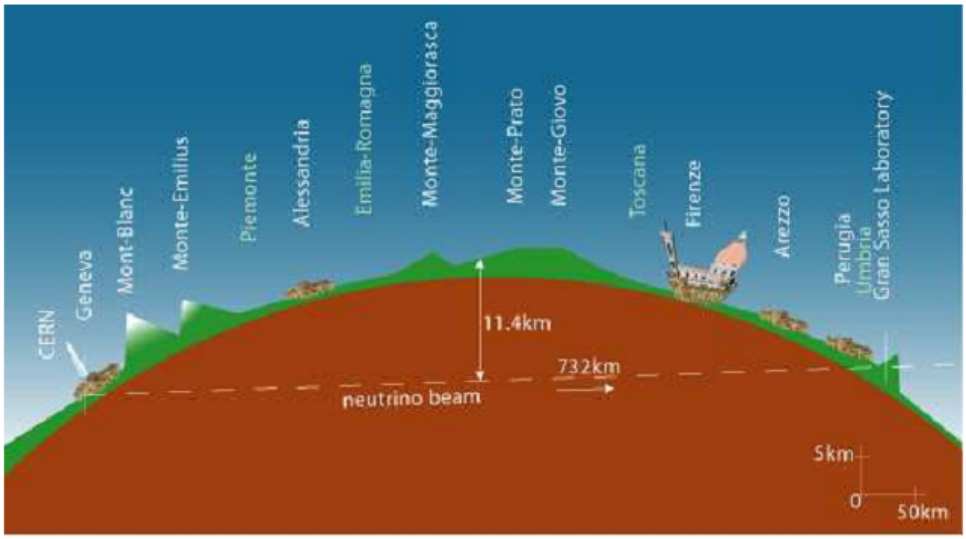

Figure 3.1: CNGS beam from CERN to LNGS [32].

reflector, in the direction of Gran Sasso. A 1 km long decay-pipe allows the pions and kaons to decay into ν_μ and muon. A schematic representation of CNGS beam is shown in Figure 3.2. The remaining charged particles (pions, kaons, protons, ...) are absorbed in a Hadron Stopper. Only neutrinos and muons are able to cross this part. The muon detectors follow the Hadron Stopper. They are used to monitor the beam and measure the neutrino beam intensity [35, 36].

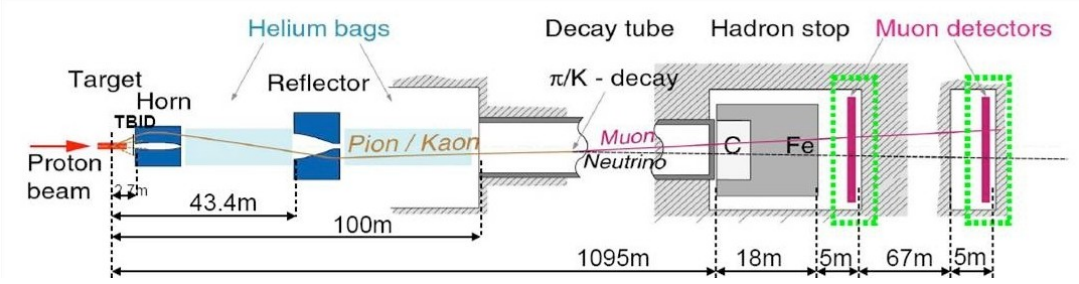

Figure 3.2: Layout of the CNGS beam line [37].

3.2 Structure of OPERA Detector

The OPERA detector is made of two identical Super-modules, each of which contains brick walls, electronic detectors (Target Tracker), and a magnetic spectrometer. A Veto system,

composed of Resistive Plate Chambers (RPCs), is placed in front of the first Super-module. A schematic representation of the detector is shown in Figure 3.3.

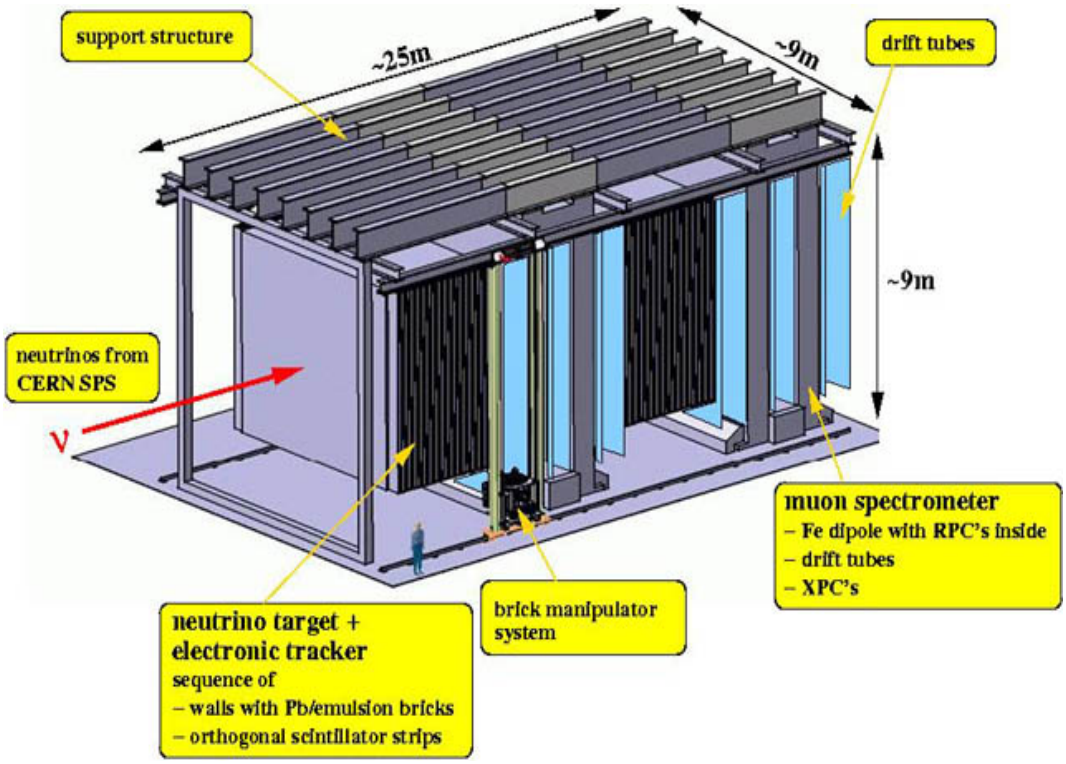

Figure 3.3: The OPERA detector [38].

3.2.1 The OPERA Brick

The OPERA target contains 150000 ECC bricks of a total mass of 1.25 kton. The total area of nuclear emulsion films used in OPERA is 110000 m^2 corresponding to 8.85 million films. Due to this large amount, it was necessary to develop an automated machine for brick assembly, which is called Brick Assembly Machine (BAM) [39, 40].

A pair of nuclear emulsion films, called Changeable Sheet (CS), is placed on downstream of the brick, which provides an interface between the brick and the electronic detectors. The Changeable Sheets can be removed from the brick and analyzed independently.

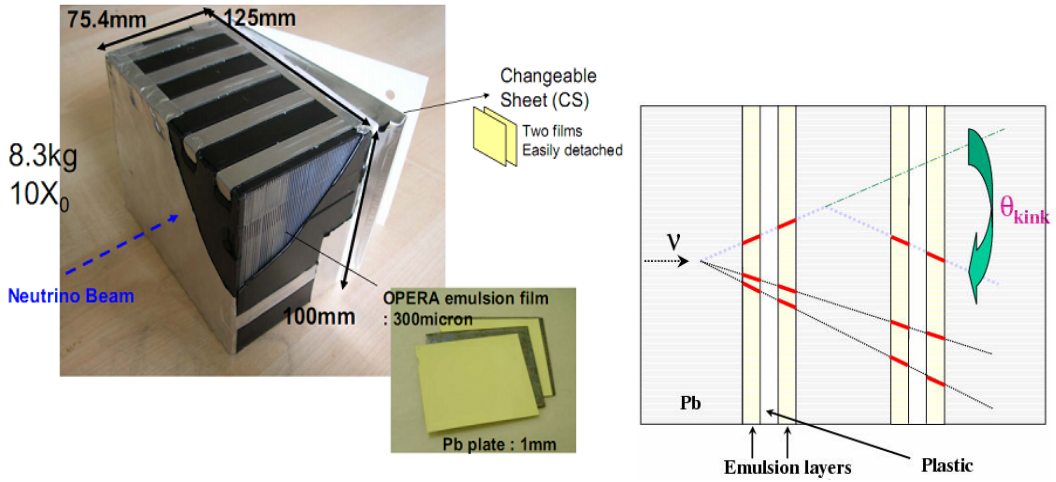

Figure 3.4: The detailed structure of an OPERA Brick [37, 41].

3.2.2 Electronic Detectors

Each Super-module is composed of 31 brick walls and 31 Target Trackers. The bricks are inserted and removed from the walls by two automatic robots, called Brick Manipulating System (BMS) and located at the sides of the detector [40, 42].

3.2.3 Target Tracker

A Target Tracker consists of 4 horizontal and 4 vertical modules that provide the x, and y coordinates of transversed charged particles. Each module contains 256 scintillating fibers 6.8 m long, 2.63 cm wide and 1 cm thick. Besides, each module reads out, through Multi-anode, and 64-pixel photomultipliers, placed at the end of the fibers as shown in Figure 3.5 [43, 44]. The main task of the Target Tracker is to locate at real-time, where the neutrino interaction occurs inside the target wall. And the CSs are used to confirm this selection and define the region of the emulsion film to be analyzed within the brick.

3.2.4 The Magnetic Spectrometers

The task of the magnetic spectrometers is to identify muon and measure its momentum. Each spectrometer is composed of two magnetized iron walls. The magnetic field inside the wall

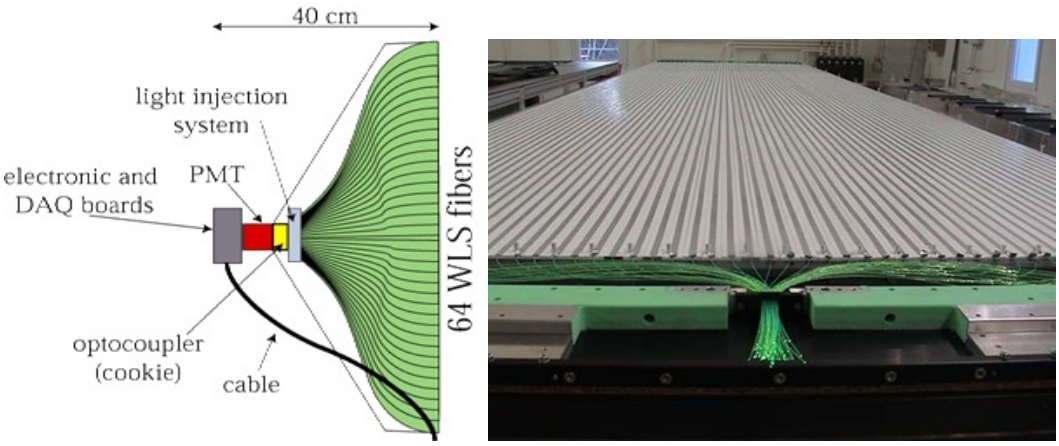

Figure 3.5: Schematic view of an end-cap of the scintillator strips module and an electronic target tracker module in construction site [45].

is essentially uniform with intensity of 1.55 T. The transverse dimensions of the magnet are around 8 m long, 8.75 m wide, and 2.64 m thick [44].

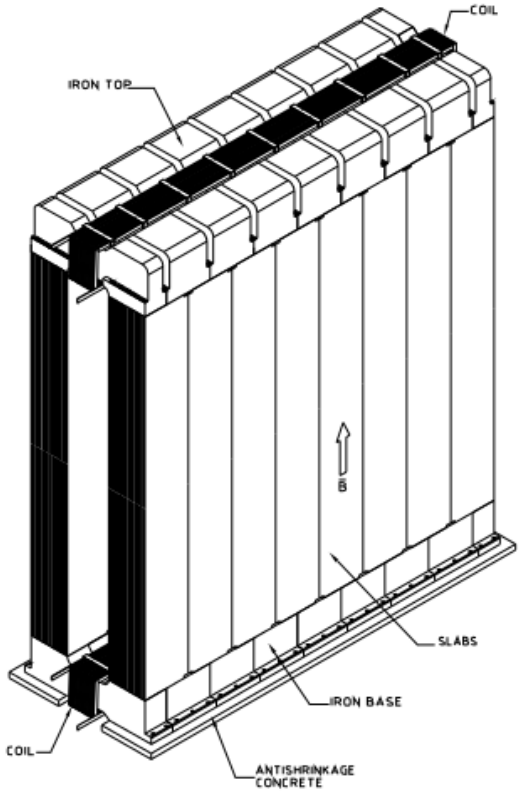

Figure 3.6: General view of the OPERA Magnet [30].

The magnets are equipped with active detectors: the iron planes are interleaved by Resistive

Plate Chambers (RPCs, Inner Tracker) and high precision tracking (Precision Tracker, PT) detectors which are placed in front of, behind and inside the magnet. The Precision Tracker (consisting of vertical planes of drift tubes) with the other parts of the muon spectrometer are used for the muon identification, the definition of the sign of the muon and its momentum. Two HPT planes are located between the two walls of the magnet in order to perform angular measurements of the muon [46, 47].

3.2.5 Veto System

The neutrinos from the CNGS can interact with external matter before reaching the OPERA detector, for example they can interact with the rock complex of the Gran Sasso and the produced particles can pass through the OPERA detector. This signal may erroneously be associated with a brick, and resulting in its extraction. To prevent this, a veto system, consisting of two layers of RPC is located in front of the OPERA detector [48].

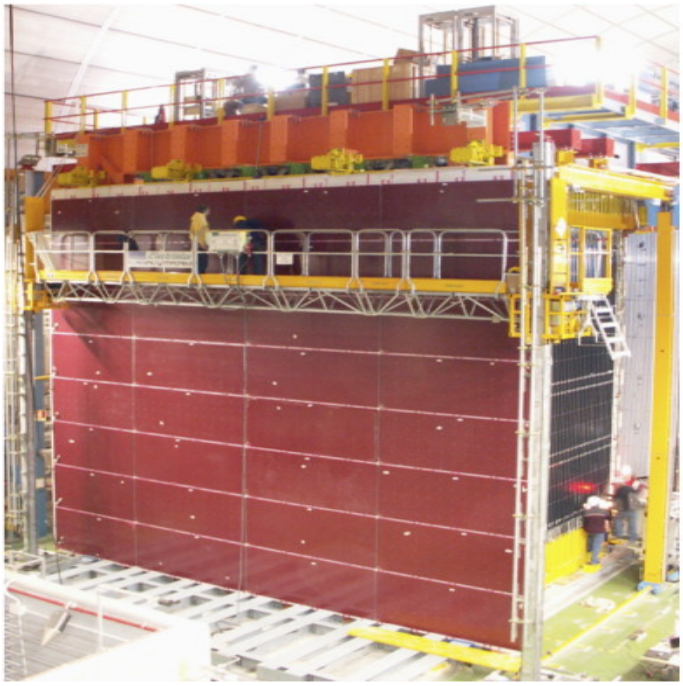

Figure 3.7: A View of VETO System [48].

3.3 Brick Handling

The synchronization between the detector and the CNGS beam is online by means of a GPS (Global Positioning System). When a neutrino interaction occurs in the detector, electronic detectors provide a trigger and event is accepted for the analysis. Then the following steps are applied in order to locate the neutrino interaction in the brick: Firstly, the data from the electronic detector are processed by a software algorithm that selects the brick with the highest probability of containing the neutrino interaction vertex [49, 50]. After that, the brick is removed from the wall by means of the BMS and then exposed to X-rays to define an intrinsic reference system. There are two independent X-ray exposure for each brick. The first one, named as CS marks, ensures a reference system between the pair of CSs and the more downstream emulsion film of brick (exposure front). The second one, named as lateral marks, produces fine marks on the sides of the brick (exposed side). It is used to keep the memory of the relative positions of the films inside the brick. After the first X-ray exposure, the pair of CS are removed from the brick and developed in the underground laboratory in Gran Sasso. Moreover, the related brick is placed in a shielded room to reduce the background due to the environmental radioactivity. If the analysis reveals traces of CS compatible with the electronic detector reconstruction, we proceed to the second X-ray exposure for the brick. Then, the brick is exposed to cosmic rays about 12 hours in order to collect enough number of cosmic muons to improve the alignment of films. Consequently, the emulsion films of brick are developed and distributed in different scanning laboratories in Europe and Japan [50].

3.4 Analysis of Neutrino Events

The proof of the $\nu_\mu \rightarrow \nu_\tau$ oscillations in the OPERA detector is identification of ν_τ Charged Current (CC) interaction.

$$\nu_\tau + N \longrightarrow \tau^- + X. \tag{3.1}$$

Since the rate of expected events is very low, it is crucial to identify ν_τ CC events with a high efficiency from those induced by neutrinos of different flavor i.e. ν_μ. Given the energy spectrum of the CNGS neutrino beam, the expected average flight length of τ-lepton is about

450 μm and the τ-lepton decays through the following decay topologies [52]:

$$\tau^- \longrightarrow e^- \nu_\tau \overline{\nu}_e, \qquad (BR = 17.8\%) \tag{3.2}$$

$$\tau^- \longrightarrow \mu^- \nu_\tau \overline{\nu}_\mu, \qquad (BR = 17.4\%) \tag{3.3}$$

$$\tau^- \longrightarrow h^- h^+ h^- (n\pi^0)\nu_\tau, \qquad (BR = 15.2\%) \tag{3.4}$$

$$\tau^- \longrightarrow h^- (n\pi^0)\nu_\tau. \qquad (BR = 49.5\%) \tag{3.5}$$

The decay topologies are classified according to the position of decay vertex. If the neutrino interaction and the τ-lepton decay vertices are in the different plates, the decay topology is called "long-decay." On the other hand, if both vertices are in the same plate, it is called "short-decay." The short decay can identified by measuring the Impact Parameter (IP) of tracks as shown in Figure 3.8 [52, 51].

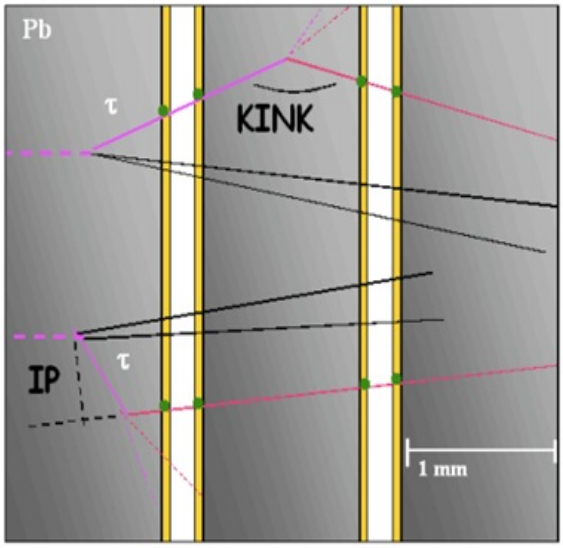

Figure 3.8: View of long decays (top) and short decays (bottom) [51].

The identification of τ-decay topologies requires kinamatical selection in addition to topological identification of the decay. The most efficient channel is $\tau \rightarrow e$ channel. This channel is almost background free if the electron shower is identified. The second clear topology is $\tau \rightarrow \mu$ channel. In this channel muon is identified by muon spectrometer with a high efficiency. The main background for this channel is the large angle scattering of muon which is produced in ν_μ CC interactions. Although the hadronic channels occupy large branching

channel, they are suffered from large background due to elastic scattering or secondary interactions of the hadrons in the ECC brick. In order to suppress topological backgrounds, a set of kinematic cuts which are given in Table 3.1 are applied [52].

Table 3.1: Kinematic cuts.

τ-decay	kinematic cuts
$\tau \rightarrow e^-$ channel	Energy for τ daughter should be greater then 1 GeV.
$\tau \rightarrow \mu$ channel	Muon momentum should be between 1-15 GeV.
$\tau \rightarrow$ h channel	Muon momentum should be greater then 2 GeV.
$\tau \rightarrow$ h channel	The kink angle must be greater than 20 mrad.
$\tau \rightarrow$ h channel	The total transverse momentum (PT) must be greater than 600 MeV/c.

The neutrino events satisfying both topological selection and kinematical cuts are the candidates for ν_τ appearance.

CHAPTER 4

AUTOMATIC EMULSION MICROSCOPE AND EMULSION SCANNING

In the OPERA experiment, about 30 events per day must be analyzed and for each event about 200 cm^2 area of emulsion film are scanned. This requires a high speed scanning system in order to complete the measurements in a reasonable time.

In the OPERA experiment emulsion scanning has been performed by fully automatic scanning systems. There are basically two types of systems: one developed in Japan, at Nagoya University [52], the other one, European Scanning System (ESS), developed by the collaboration between European laboratories [53]. In the following section, the main components and parameters of the ESS are described in detail.

4.1 European Scanning System and Emulsion Scanning

The main components of the ESS microscope mentioned above, shown in Figure 4.1, are:

- A support table (MICOS) which has high quality mechanics.
- Computer driven horizontal and vertical stages.
- A granite arm as a supporting frame for CCD camera and objective.
- A mega-pixel CCD camera (CMOS) mounted on the vertical plate on the granite arm. It is interfaced with a frame-grabber and vision processor.
- Optics and light system (NIKON) located below the scanning table.

The scanning speed of the European Scanning System is 20 cm^2/h.

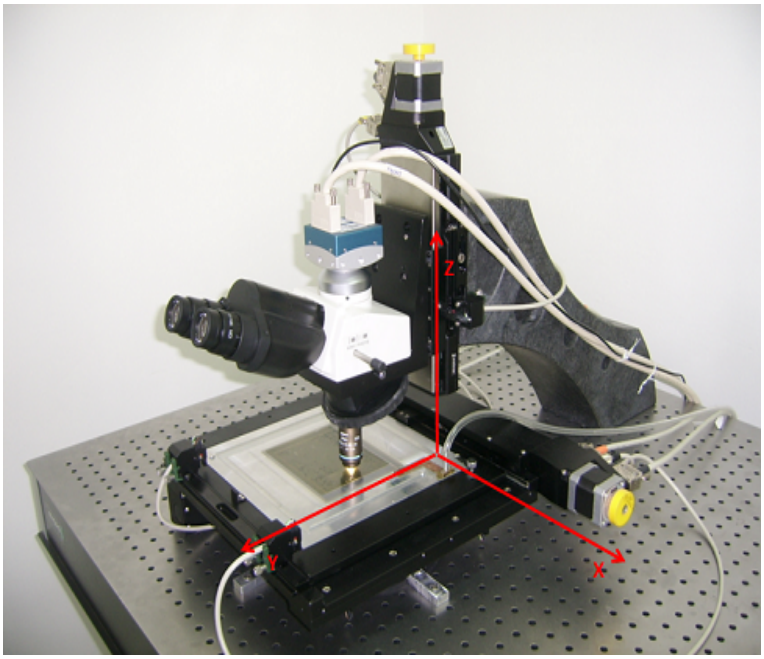

Figure 4.1: ESS scanning microscope.

During the scanning, objective focuses at different depths of emulsion film and take tomographic images. In total 15 tomographic images are taken over 44 μm thick emulsion layer. These images are sent to Odyssey board for processing. The camera has a capability of working with a rate of 660 MB/s. In addition, OPERA uses the frame rate of 376 frames per second, which corresponds to 496 MB/s (Figure 4.3).

The first step of image tracking is to reconstruct micro-tracks using aligned clusters of dark pixels. Then micro-tracks at both sides of plastic base is connected to form the base-tracks (Figure 4.4).

The final step of processing is to reconstruct particle tracks by connecting the base-tracks in consecutive emulsion films.

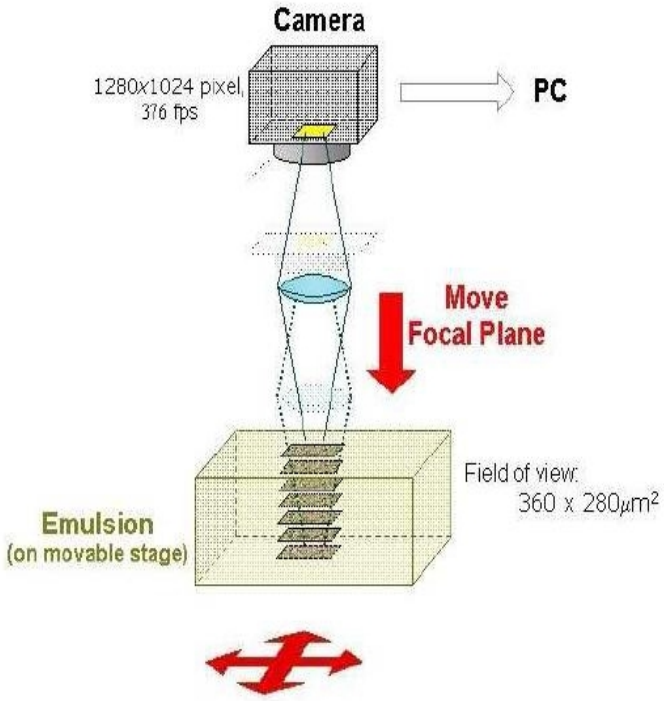

Figure 4.2: Taking a series of successive images in different depths of the Emulsion [54].

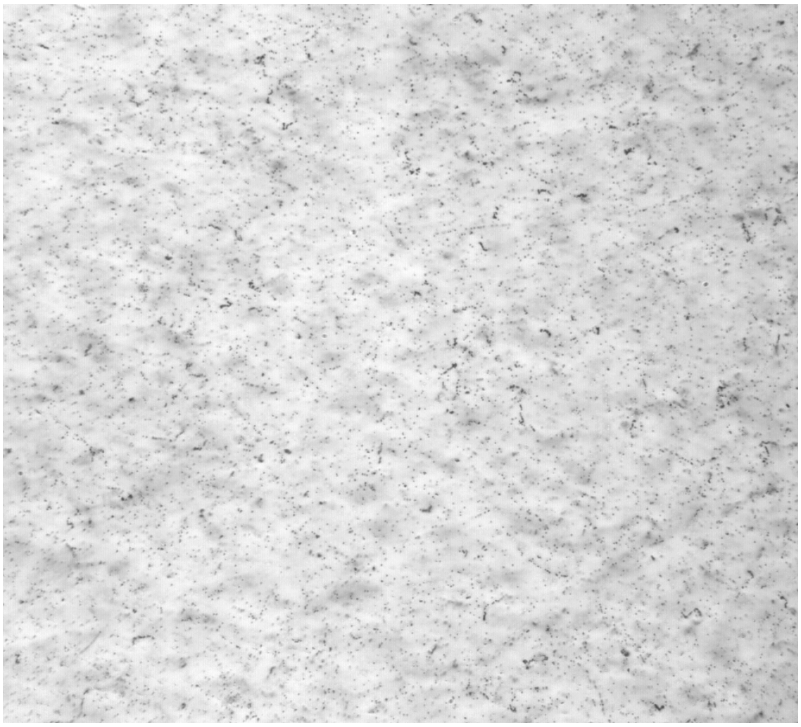

Figure 4.3: The Emulsion view from Ankara Scanning System.

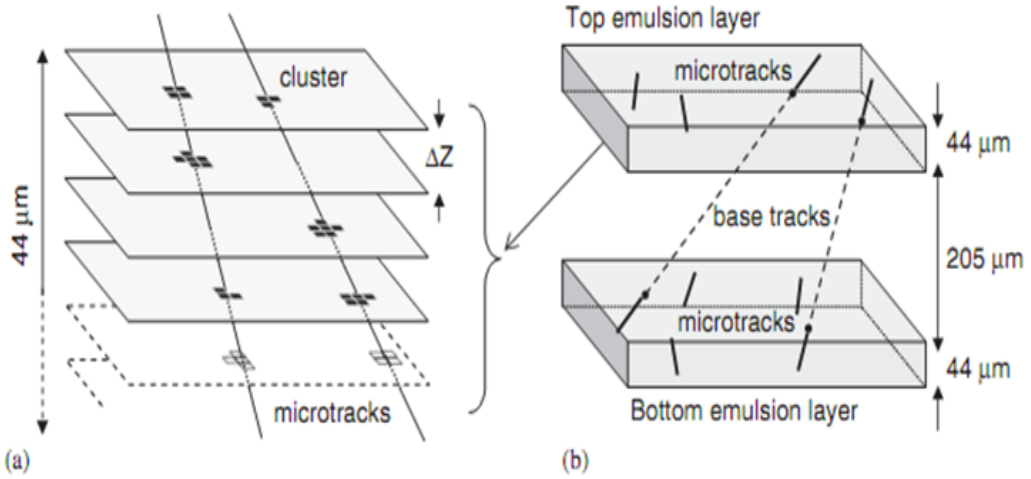

Figure 4.4: a) The reconstruction of micro-tracks in an emulsion layer b) The combination of micro-tracks through the plastic base forms the base-tracks[55].

4.1.1 SySal Software

The SySal software, written in C++, was developed by Cristiano Bozza from the OPERA Collaboration.

Some important features of the SySal are given below:

1) Opera Batch Manager: The part of the software that is responsible for managing the scanning.

2) Vertigo Scan Server: This part is responsible for writing the data to the database while scanning.

3) Scan Server: This is the main program runs at microscope workstation and is responsible for collecting and arranging the data during the scanning.

4.1.2 Database

In Emulsion Scanning Laboratory in METU, there is a permanent connection with OPERA database located in Lyon. By running Oracle SQL, it is possible to reach the information about OPERA events like position and angle information of the particle tracks found in CSs.

4.2 Scanning Efficiency of Ankara Scanning System

In terms of scanning results and tracking efficiency, there should be a standardization between different labs in the OPERA Experiment. It means that every scanning result coming from different labs should have the similar efficiency. In order to monitor the scanning efficiency of each lab, a set of nuclear emulsion films were exposed a pion beam at CERN. Then these films are distributed to different emulsion scanning labs.

We have received 6 emulsion films which are scanned and analyzed with our scanning system. Figure 4.5 shows our tracking efficiency plot. The mean efficiency is around 75%. Figure 4.6 shows the tracking efficiency of Bern University. Comparing the tracking efficiency of Bern system and our system, we have seen that both labs have similar scanning performance in terms of efficiency.

It is observed that they are consistent with each other.

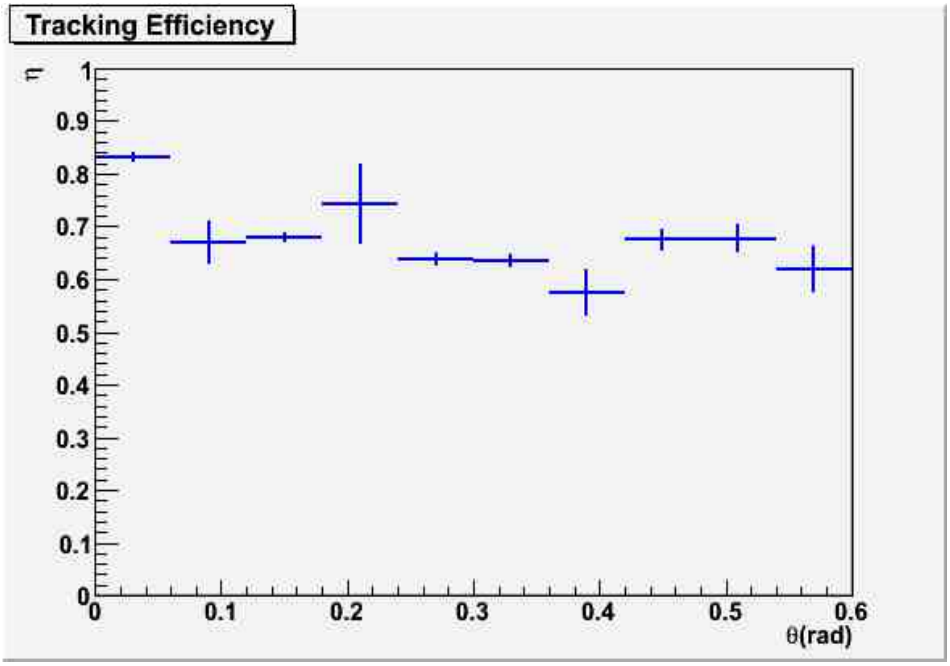

Figure 4.5: The tracking efficiency as a function of track slope (Ankara data).

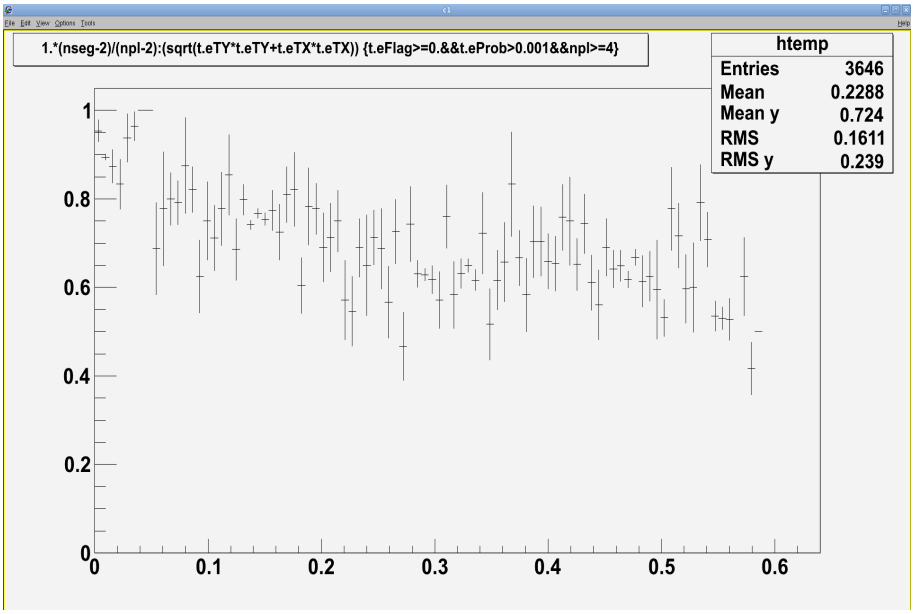

Figure 4.6: The tracking efficiency of Bern scanning system.

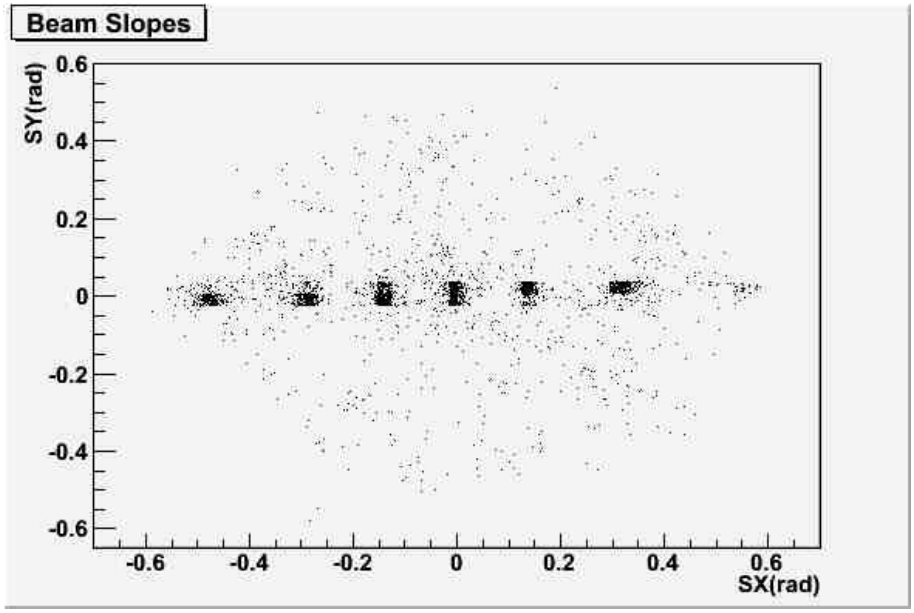

Figure 4.7: Beam slopes.

4.3 Brick Scanning

Once the OPERA brick is received, some tests have been done on brick's emulsion films. The aim of these tests was to find a specific coordinates at any plate. This is important since the events looked for, are in micron scale.

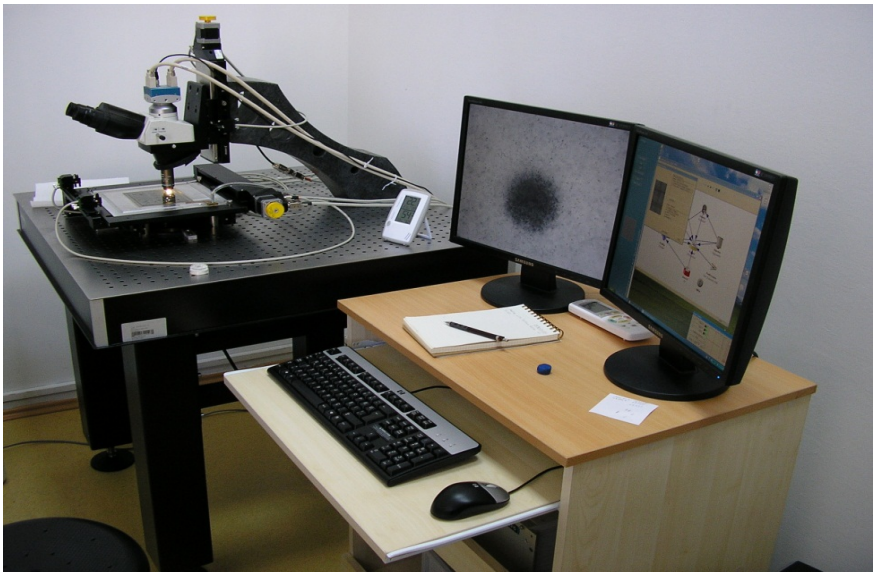

Figure 4.8: The Ankara scanning microscope.

For that purpose, there is a checking mechanism with two types of marks. First one is the CS marks. These point-like marks are found only in the last plate (numbered 57) of every brick set as shown in Figure 4.9. Although there are usually five of these CS marks, it is enough to find only four of them automatically to initiate the scanning. There are also lateral X-Ray marks, horizontal, and vertical ones, found on every plate (see Figure 4.10). These lateral marks, are located close to the corners of the emulsion film. By finding and saving the coordinates of these intersection points, the system can define a coordinate system for every emulsion film. Then these information is used for the plate alignment during the reconstruction phase. With this procedure, the software can combine the data sets taken from single plates, and construct the track of a particle passing through several plates for instance.

4.4 Event Analysis With Ankara Scanning System

Ankara microscope was assembled in September 2011 and after certain tests, the microscope was ready for the brick analysis in the OPERA experiment. As a real exercise some OPERA bricks are received and scanned.

As a first trial of event location, we scanned a brick which was already analyzed by Napoli Group in the collaboration. Considering this as “Napoli Brick”, the aim was to reproduce their

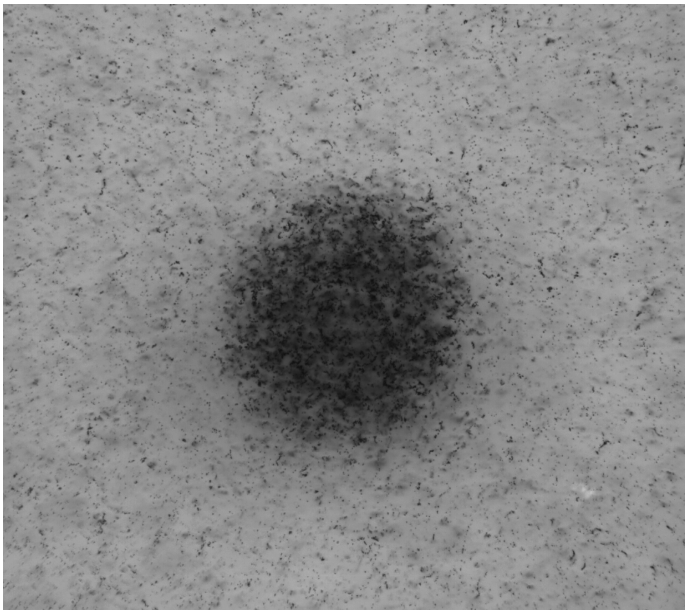

Figure 4.9: An example of CS marks in CS plates and plate ♯57.

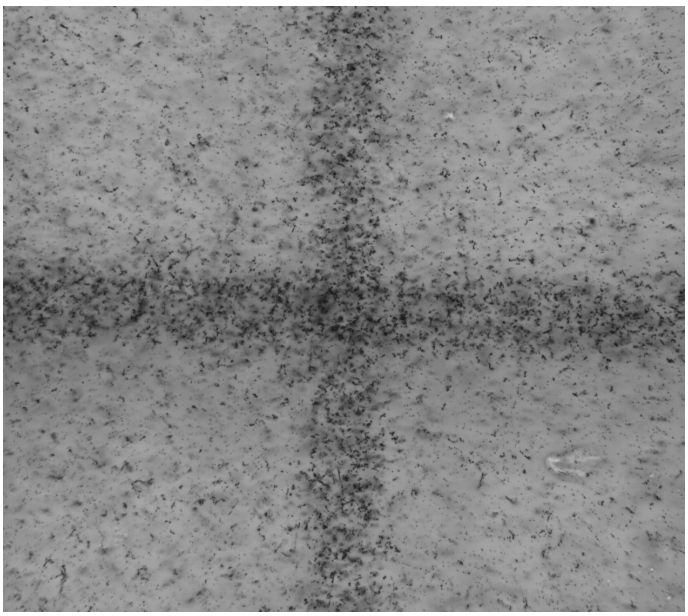

Figure 4.10: An example of lateral marks in all brick plates.

analysis results. This would provide a test whether we are capable to reproduce the analysis result of another lab.

As a first step: CS-brick connection has been done successfully by scanning 10 plates (from 57 to 48). The muon track was found in 10 plate of the brick films. Then, this track is fol-

lowed back in the brick in order to locate vertex plate. This scan-back location is performed by scanning 5×5 mm^2 area around the track position in 57 emulsion films. The data is analyzed using SySal reconstruction tools to find the vertex plate. After finding the vertex plate, a third phase of scanning is launched, the aim of this scanning is to reconstruct the neutrino interaction vertex and also search for decay vertices relating with the same neutrino event. A volume which is made of 1×1 cm^2 transverse area and 15 plates (10 plates downstream and 5 plates upstream, of the vertex plate) is scanned. After the scanning, the data is reconstructed by SySal reconstruction. Then, finally we have successfully located the neutrino interaction vertex. Our reconstruction is consistent with Napoli analysis in terms of track multiplicity at vertex and position and slopes of the vertex tracks. The information about the located event is given in Table 4.1. The reconstructed neutrino event is shown in Figure 4.13.

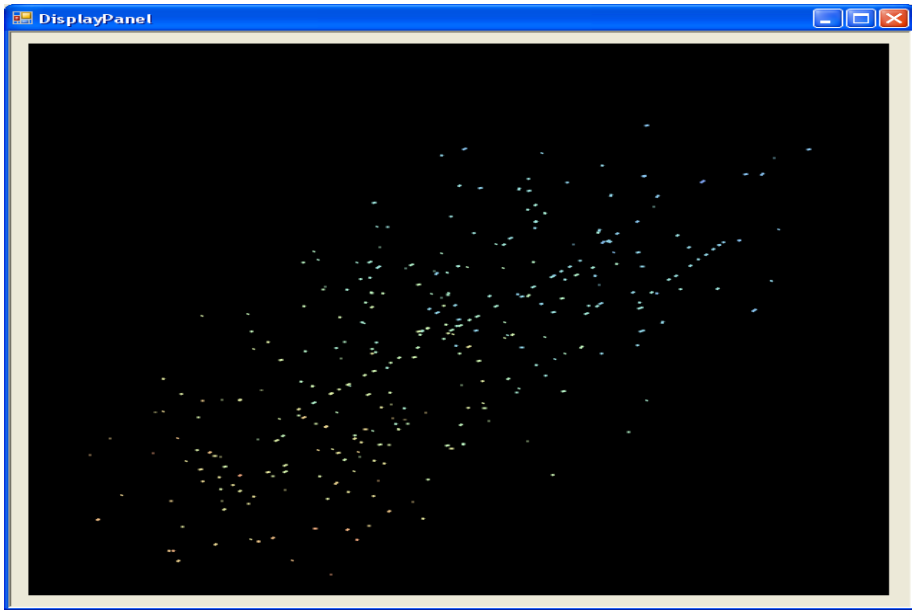

Figure 4.11: Reconstructed muon track in the brick.

Table 4.1: Vertex Data (Last entry does not related to vertex).

Track	*X*	*Y*	*Z*	*SX*	*SY*	*IP*	D_IP	*DZ*
♯1809	60497.0	33774.9	0.0	-0.0752	0.0592	1.1	2.3	898.4
♯18591	77590.2	37926.1	0.0	-0.2388	0.1354	1.1	2.3	898.4
♯15016	64504.3	30627.1	0.0	-0.0687	0.1006	-	-	-

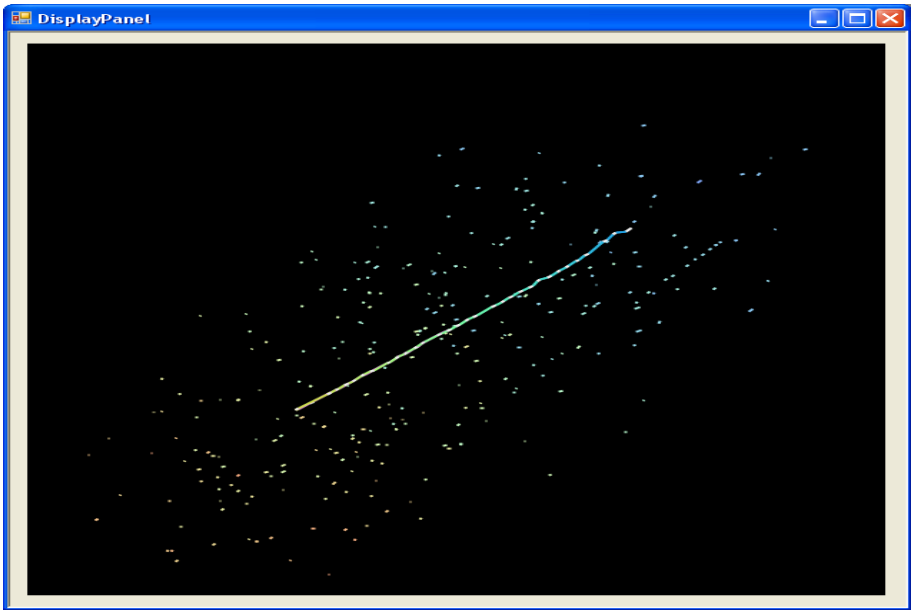

Figure 4.12: Muon track.

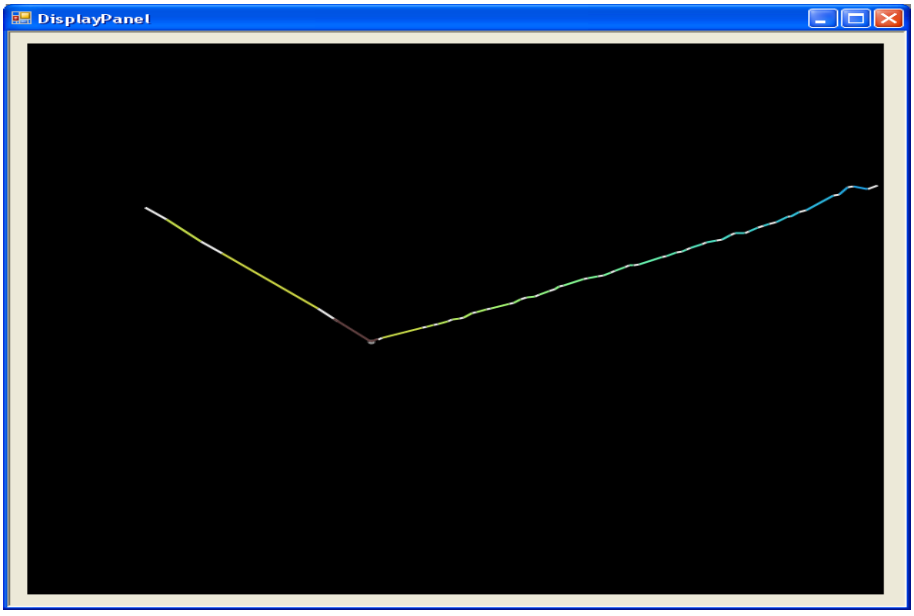

Figure 4.13: Vertex view.

After the scanning and analysis of “Napoli brick”, we have received six bricks from 2011 run. These bricks have not been analyzed before. Therefore, we call them as “Ankara bricks.”

In the following we present, the analysis of these events.

4.4.1 Event ♯11143034579

Event ♯11143034579 was one of the OPERA event assigned to the Ankara laboratory in 2012. According to the electronic detector reconstruction, this event is neutral current interaction. This is clearly visible in the electronic detector display, that there is no reconstructed muon in the detector (Figure 4.14).

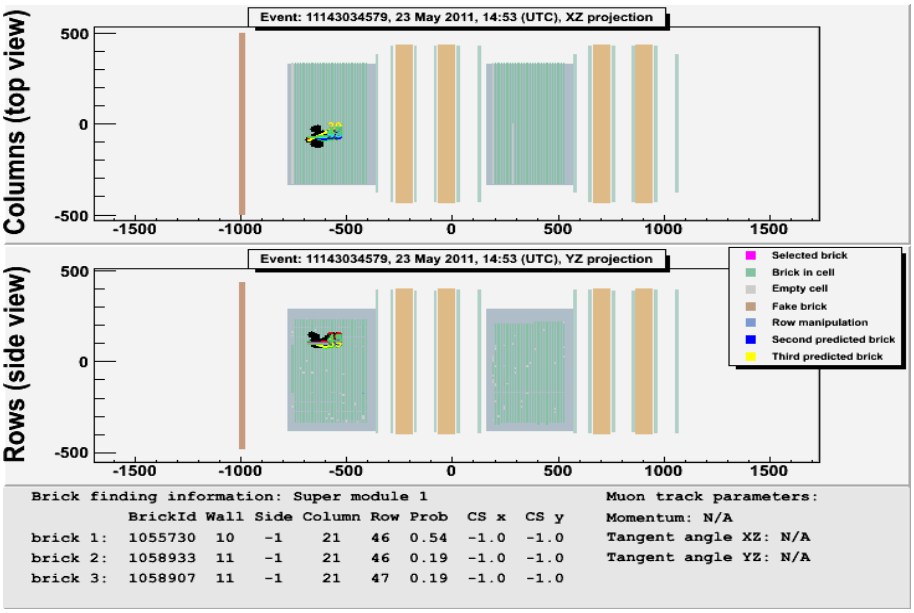

Figure 4.14: Display event ♯11143034579 in the entire detector, reconstructed by electronic detectors.

As a first step, CS-brick connection has been done successfully. Two tracks were found, and in order to locate the vertex plate, these tracks are scanned back in the brick. The analysis of scan-back data shows that neutrino vertex is located in plate 52. This means, these two tracks are stopped in plate 52. The minimum distance between these two tracks is about 2 μm. The vertex plate is also confirmed by eye checked; tracks are searched in plates 53 and 52. Both tracks are seen in plate 53, however, they are not found in plate 52. This confirms the vertex plate as 52. Figure 5.3 shows vertex and related segments around the vertex position. After manual check, we confirmed that vertex contains two tracks as shown in Figure 4.36.

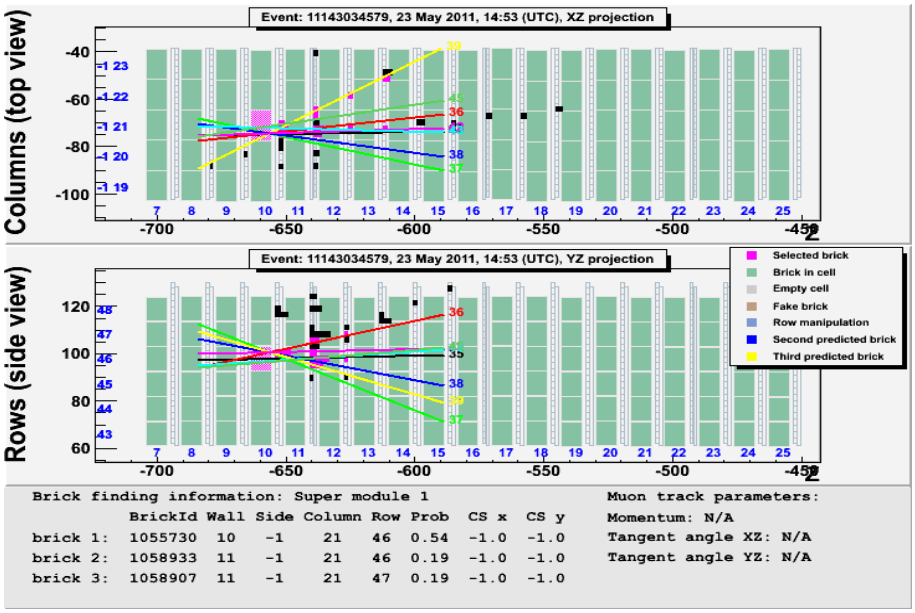

Figure 4.15: Zoom of the detector where the interaction took place (is highlighted in pink).

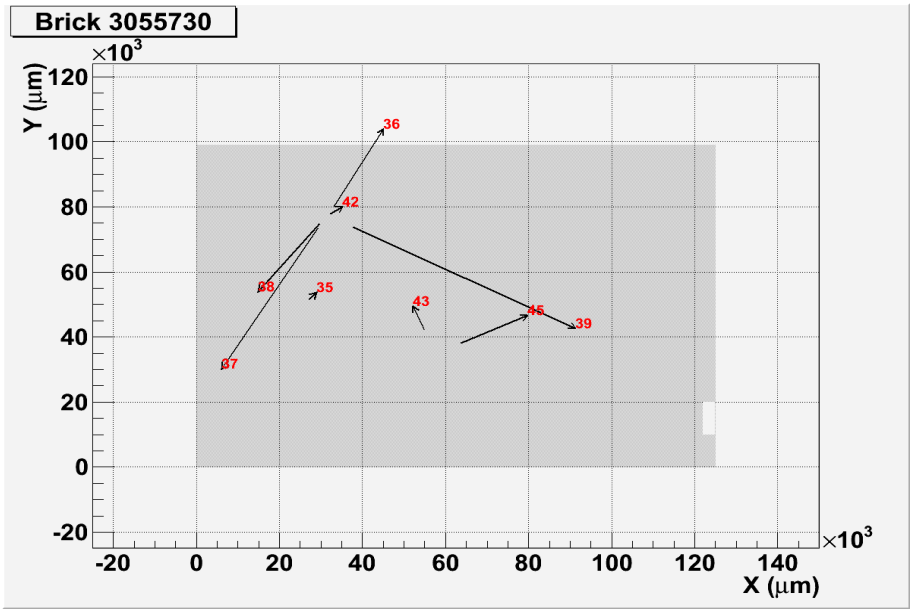

Figure 4.16: The track positions found in the CS for the event ♯11143034579. The difference of direction and the magnitude of the arrows comes from the difference of their slopes.

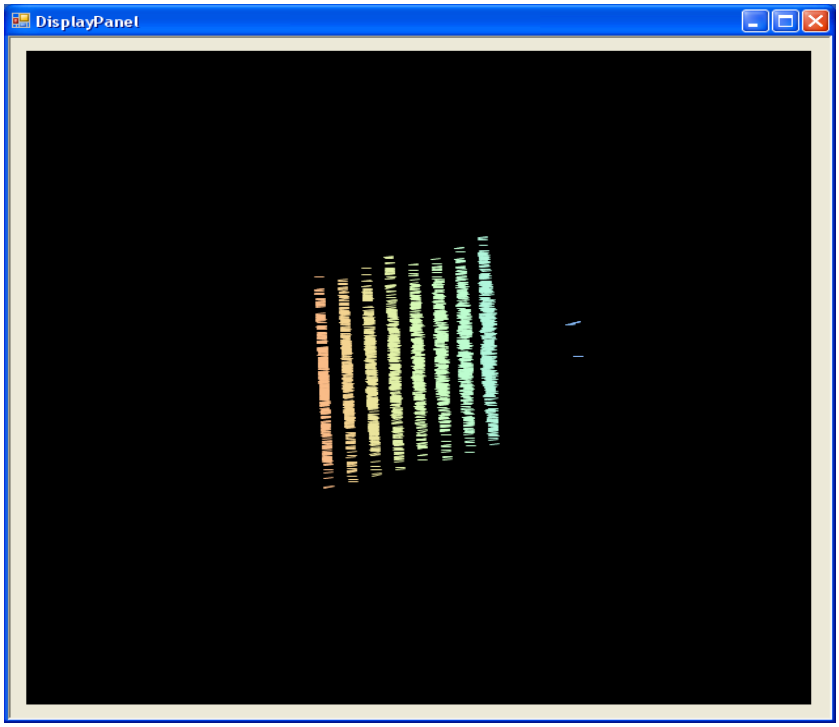

Figure 4.17: Volume scan area.

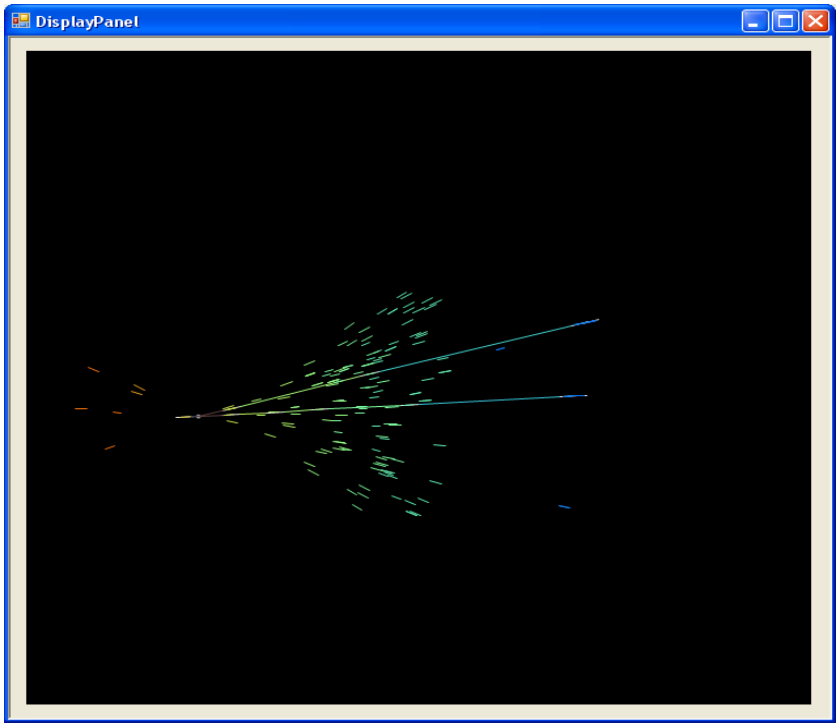

Figure 4.18: Vertex view with related segments.

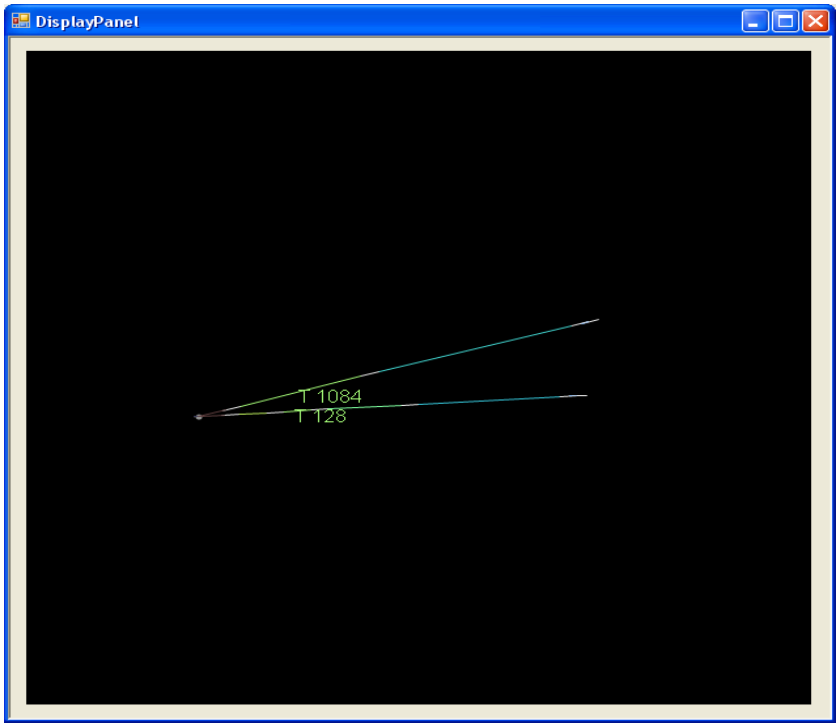

Figure 4.19: Final Vertex view.

4.4.2 Event ♯11139007521

Event ♯11139007521 was another event assigned to the Ankara laboratory. According to the electronic detector reconstruction, this event is also neutral current interaction.

For this event CS-brick connection and scan-back location have been done successfully. Figure 4.24 shows vertex and related segments around the vertex position. After manual check, we confirmed that vertex contains five tracks as shown in Figure 4.25.

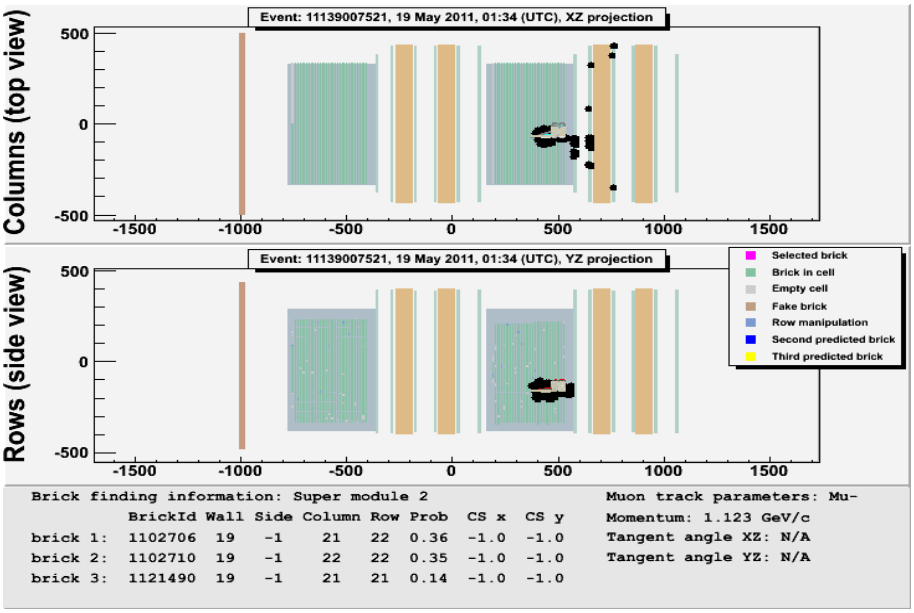

Figure 4.20: Display event ♯11139007521 in the entire detector, reconstructed by electronic detectors.

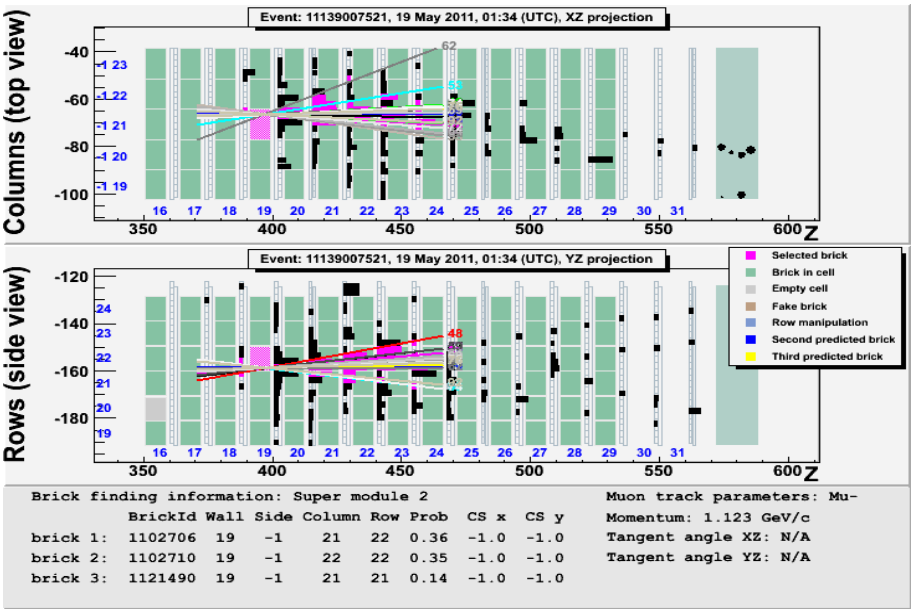

Figure 4.21: Zoom of the detector where the interaction took place (is highlighted in pink).

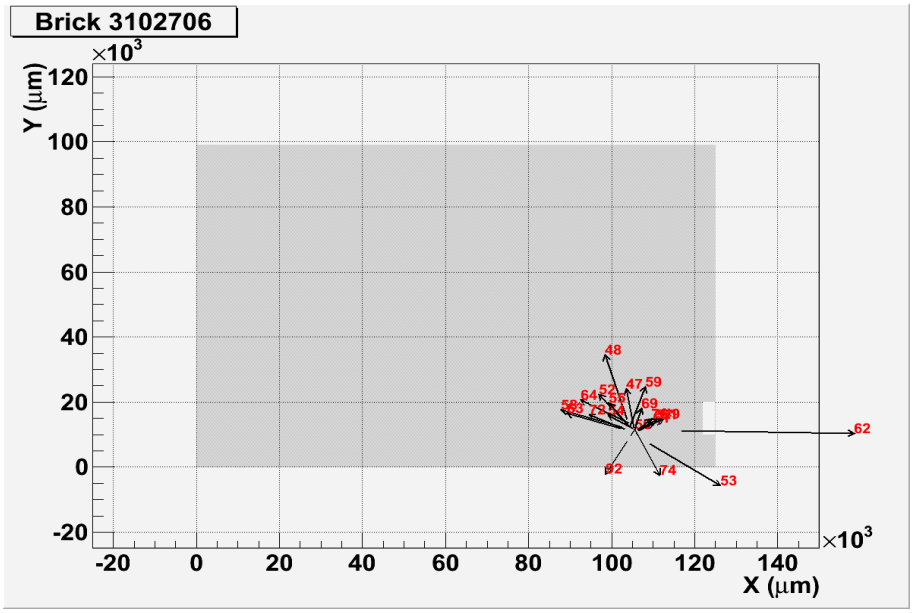

Figure 4.22: The track positions found in the CS for the event ♯11143034579.

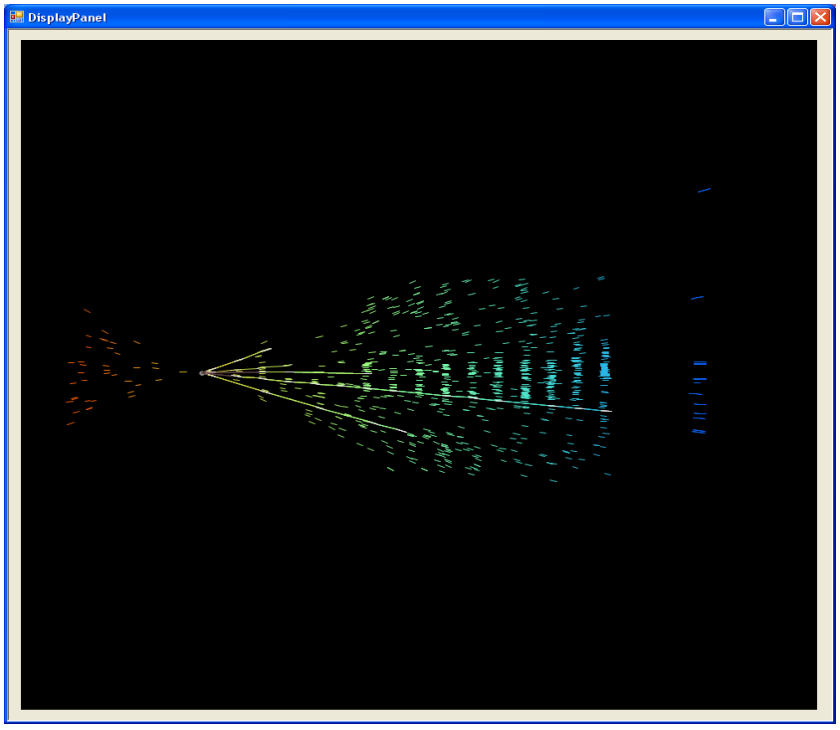

Figure 4.23: Volume scan area.

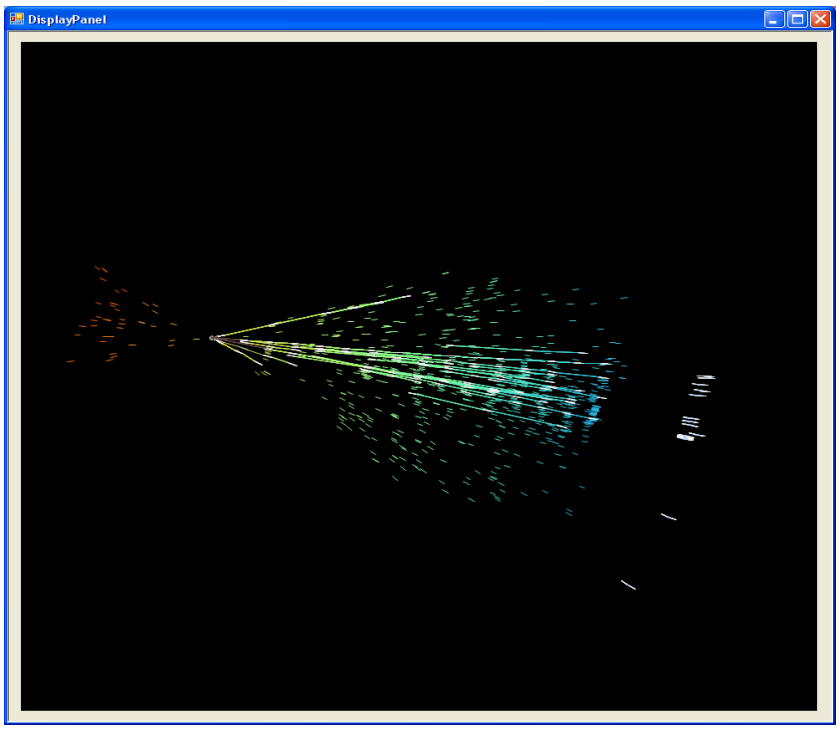

Figure 4.24: Vertex view with related segments.

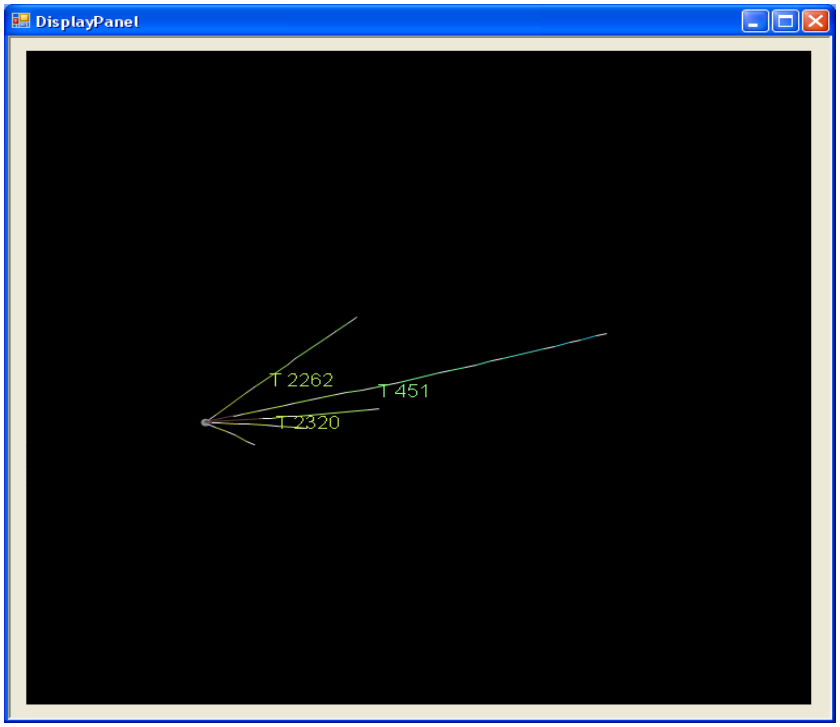

Figure 4.25: Final Vertex view.

4.4.3 Event ♯11176016909

Event ♯11176016909 is 1μ event based on the electronic detector reconstruction.

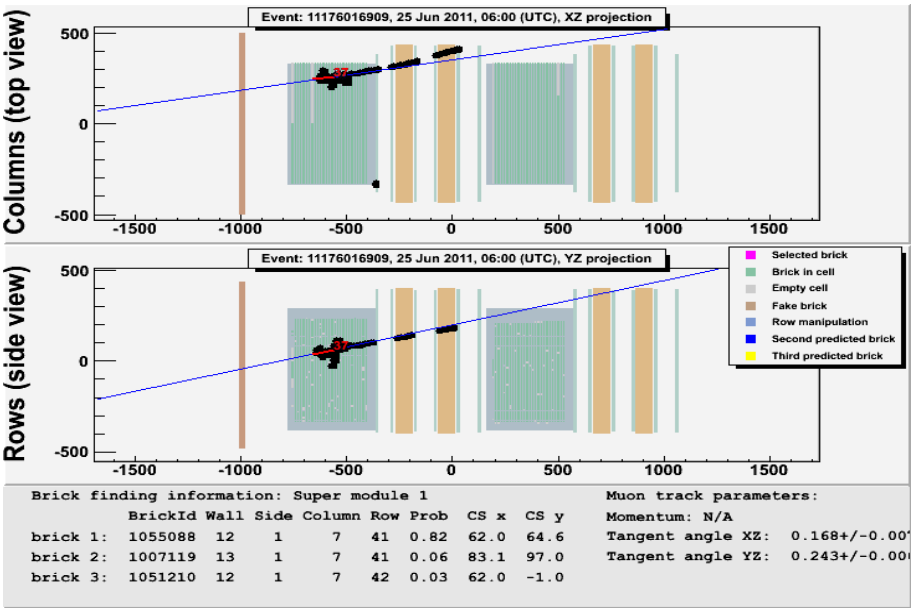

Figure 4.26: Display event ♯11176016909 in the entire detector, reconstructed by electronic detectors.

After CS-brick connection, the muon track is followed back. It was found that it stops at plate 27. After searching for vertex tracks, we confirmed that this event is one prong event.

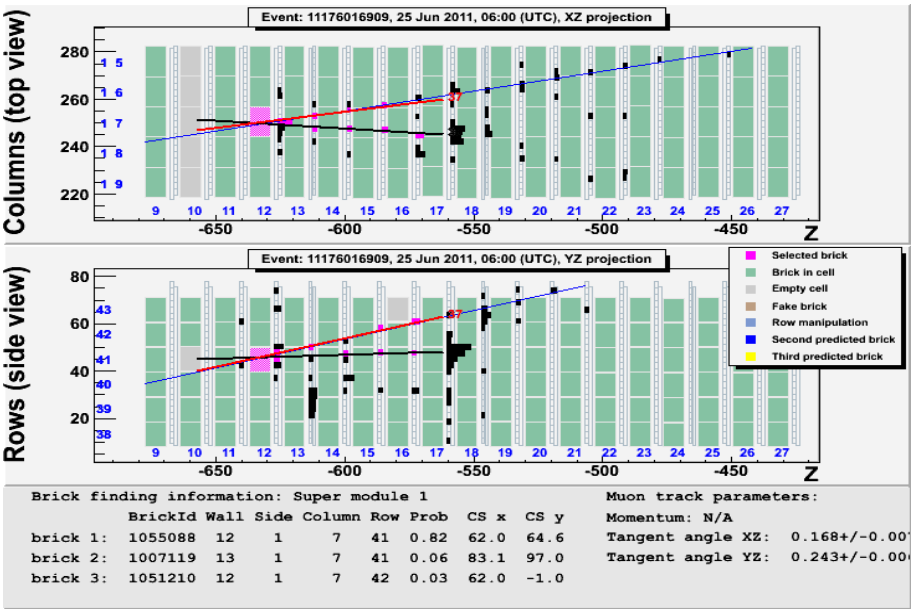

Figure 4.27: Zoom of the detector where the interaction took place (is highlighted in pink).

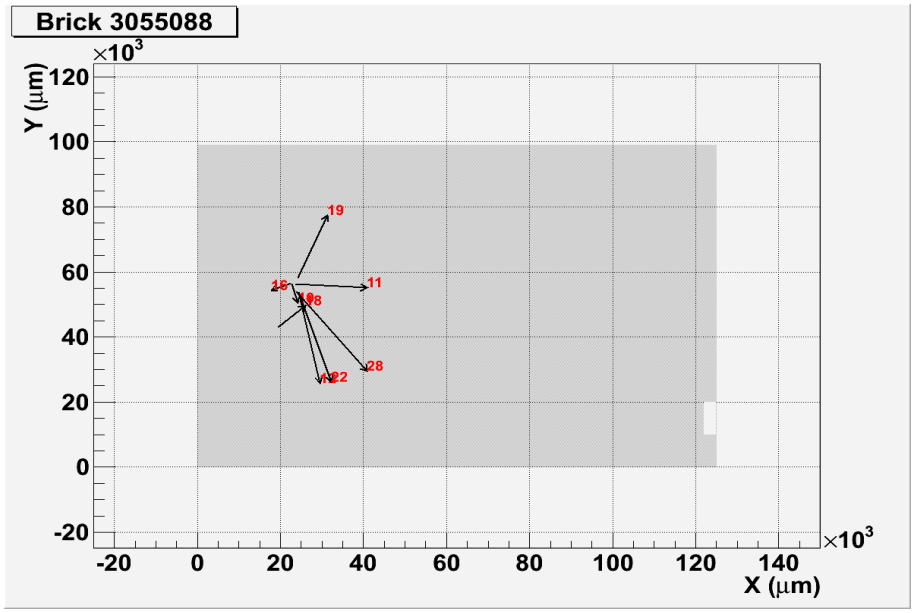

Figure 4.28: The track positions found in the CS for the event ♯11143034579.

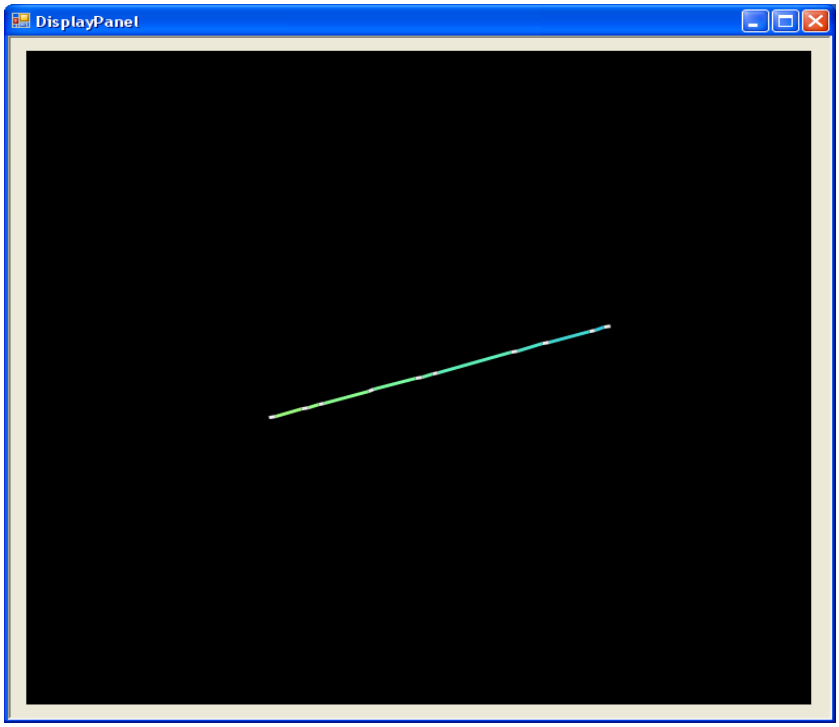

Figure 4.29: Volume scan area.

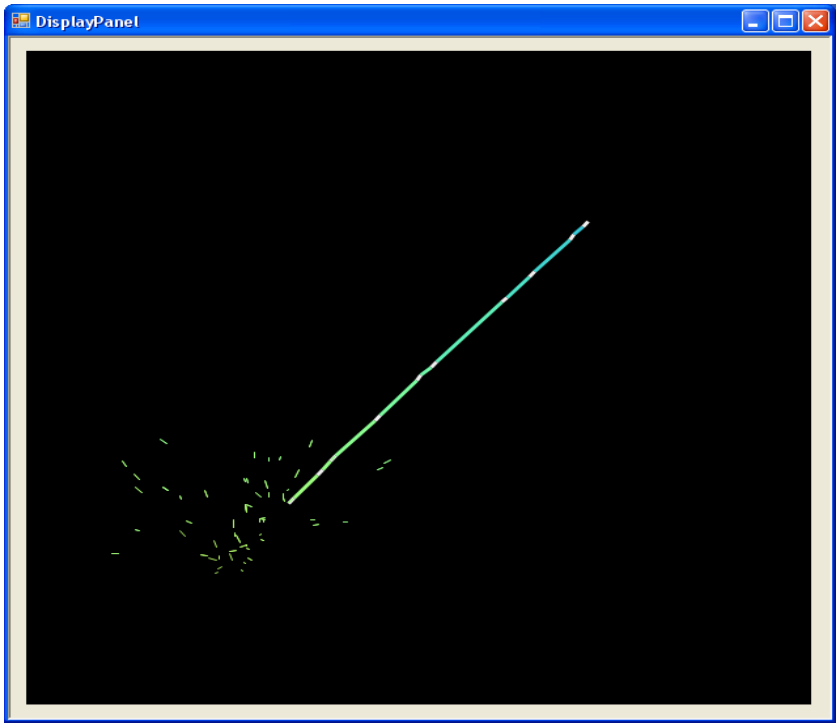

Figure 4.30: Vertex view with related segments.

4.4.4 Event ♯11256009809

Event ♯11256009809 is also 1μ event according to the electronic detector reconstruction.

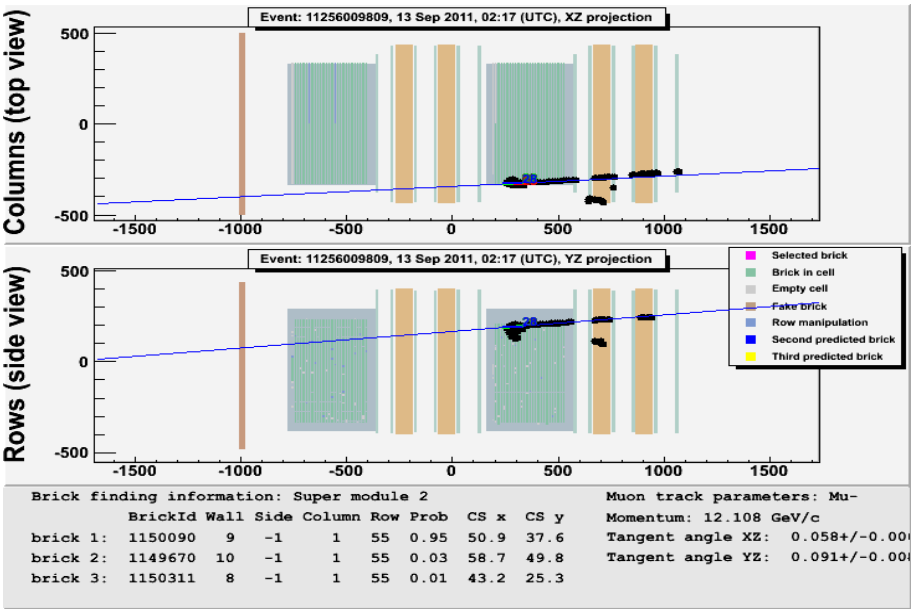

Figure 4.31: Electronic detector reconstruction for event ♯11256009809.

After CS-brick connection, the muon track was found in the brick. After scan-back scanning, we have confirmed that muon track stops at plate 46. We have searched for segments around the muon track and we have confirmed that one track is making a vertex with muon track.

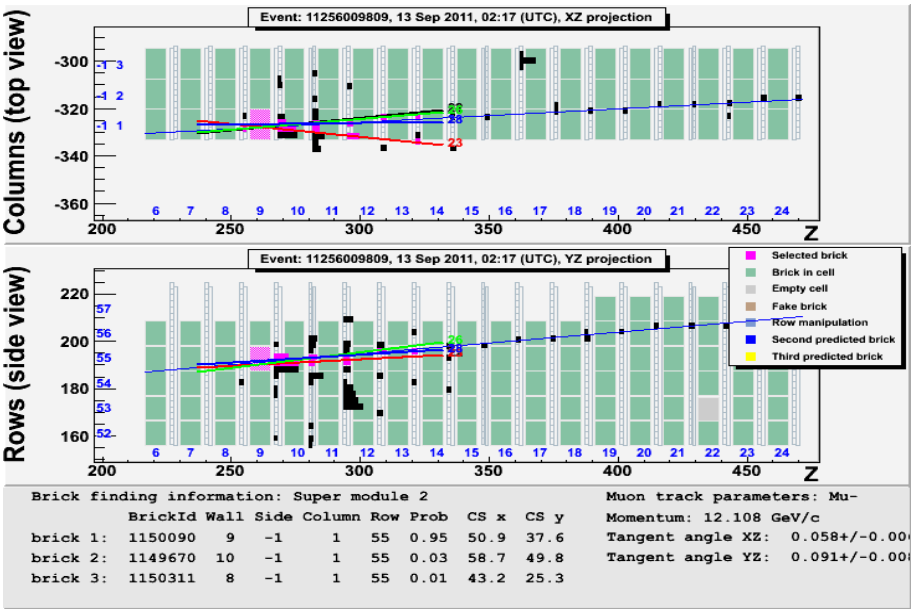

Figure 4.32: Zoom of the detector where the interaction took place (is highlighted in pink).

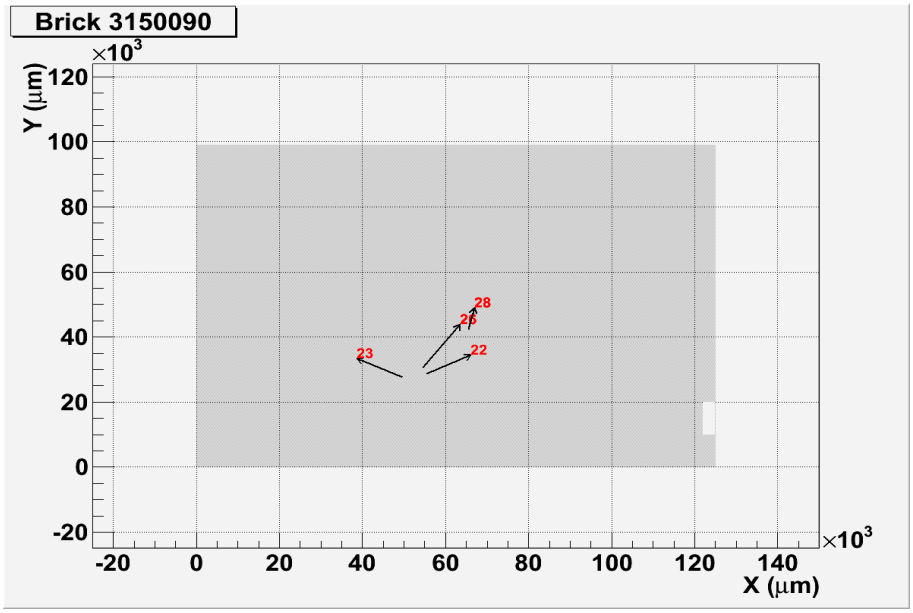

Figure 4.33: The track positions found in the CS for the event ♯11143034579.

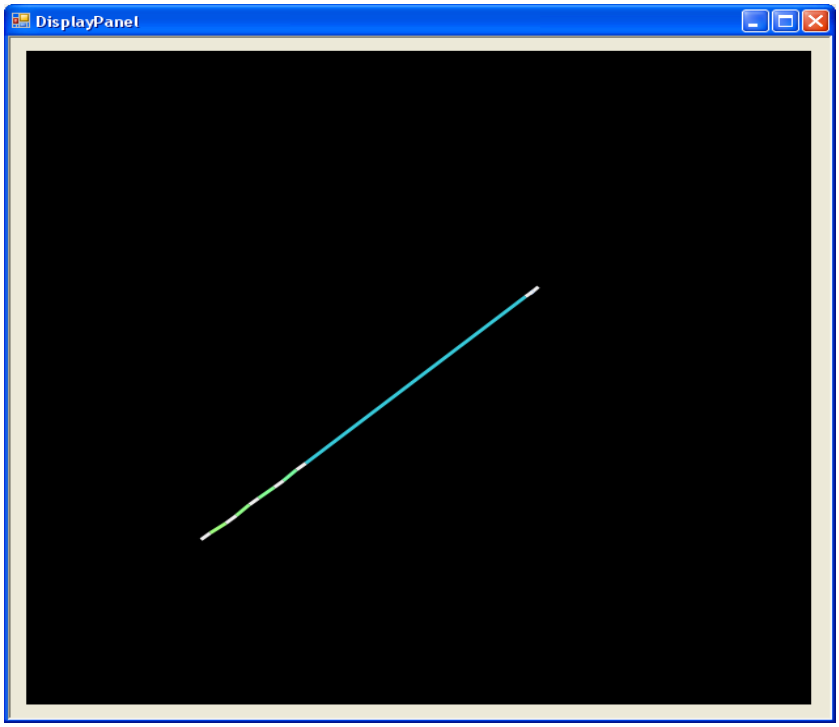

Figure 4.34: Volume scan area.

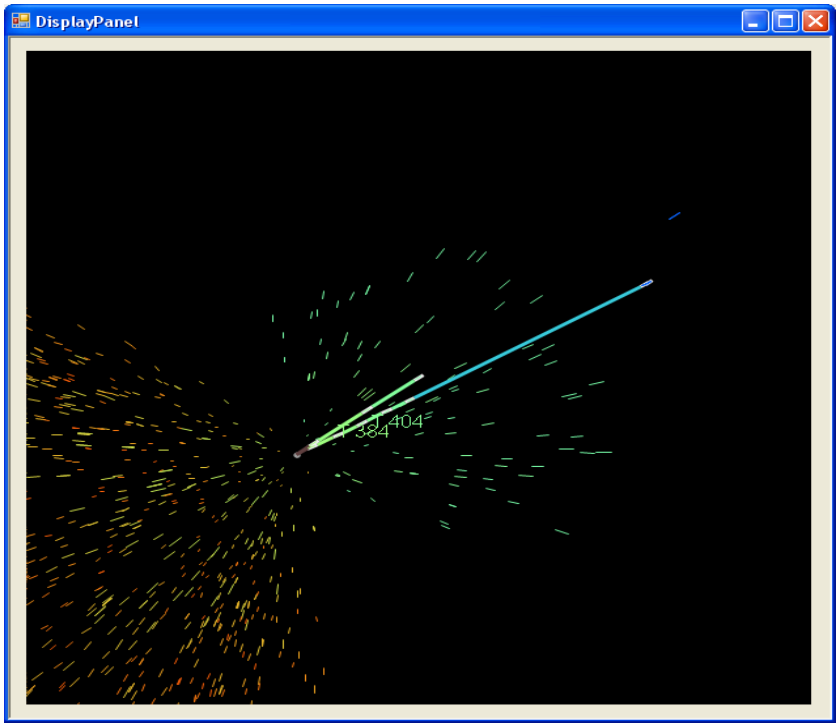

Figure 4.35: Vertex view with related segments.

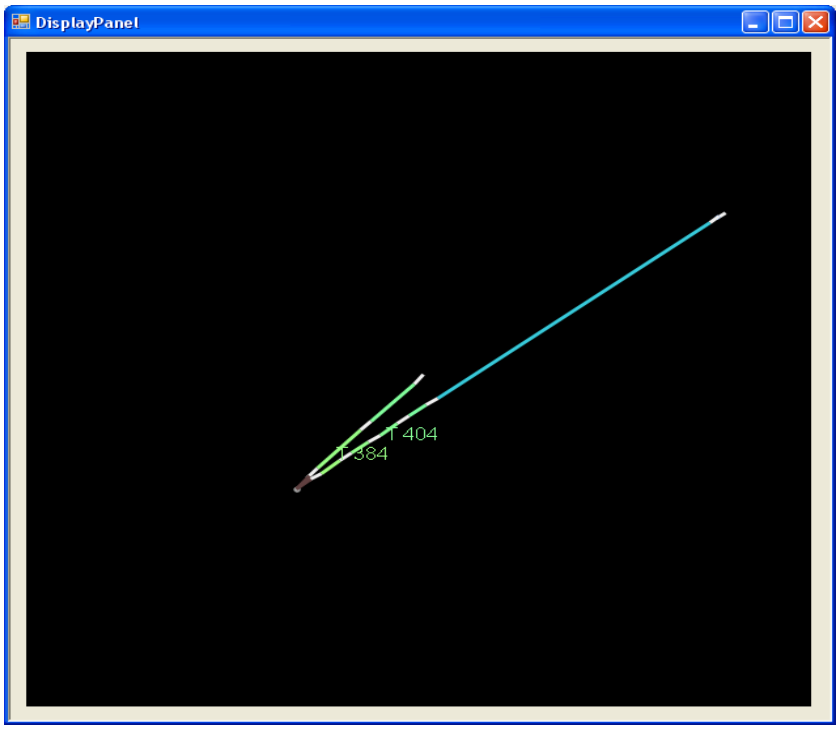

Figure 4.36: Final Vertex view.

CHAPTER 5

DATA-MONTE CARLO COMPARISONS

The comparison of Data and Monte Carlo (MC) is one of the important part of the data analysis. Since MC simulation has been used to evaluate the efficiency and background for oscillation search, it is very crucial to check whether MC simulation reproduce Data or not.

In the OPERA experiment, a software framework, called OpRelease, is developed for Monte Carlo simulation and Data analysis [56]. MC events are generated using OpNEGN package [57]. Its output is an ASCII file containing the kinematic information of particles created by neutrino interaction. Then, using a root macro, these files are converted into root files. The output of OpNGEN is considered as the input of OpEmuIo, and it generates root files as well. These generated root files involves information about emulsion data like zone, view and raw Data. After that, these output files are used as input to OpEmuRec. This software performs the event reconstruction, which can be done through different reconstruction algorithms like Fedra [58] and SySal [59] in the collaboration. For our analysis SySal reconstruction has been used. Furthermore, an analysis code for Data-MC comparison has been developed as a part of this study.

The Data reconstruction is similar to the MC case. As a first step, raw Data is processed through reconstruction algorithms in OpRelease framework in order to reconstruct the micro-tracks, which are aligned grains, inside the emulsion layer. In next step, the base-tracks are reconstructed through the connection of micro-tracks, which are detected at each layer of emulsion films (Figure 5.1). In order to reconstruct the particle tracks, emulsion plates must be aligned. An affine transformation, consisting of rotation, and shifts is applied. After that, particle tracks are formed by connecting base tracks plate by plate to reconstruct the tracks. In track reconstruction, Kalman filter algorithm is applied. After the tracking, particles are

clustered to reconstruct the vertices.

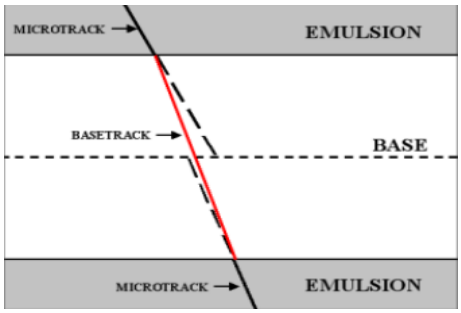

Figure 5.1: A schematic view of micro-tracks and base-track.

The reconstructed vertices are classified as primary and secondary vertices. In OPERA, the primary vertex is named for the neutrino interaction point in the brick. A ν_μCC interaction with μ^- and charged hadrons is illustrated in Figure 5.2 . In most of the ν_μCC events, there is only one vertex which is called primary vertex. However, if one of the primary particle decays in the brick, it forms the secondary vertex (Figure 5.3).

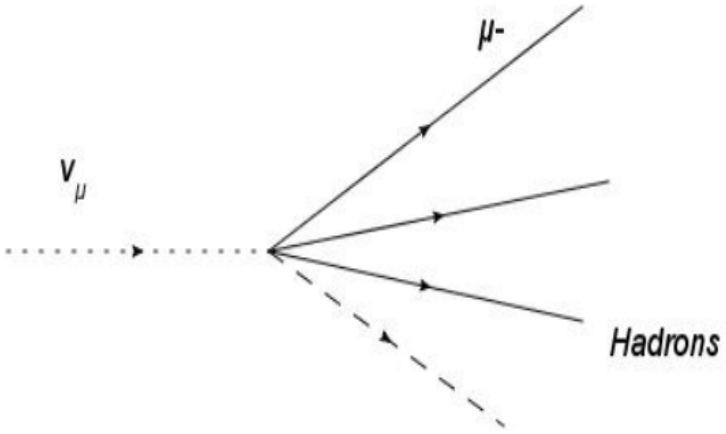

Figure 5.2: ν_μCC interaction with one vertex.

In the following, we present the result of Data-MC comparisons for ν_μCC and ν_μCC-charm events. For this study 1000 ν_μCC and 1000 ν_μCC-Charm Monte Carlo events are used. MC events are produced using OpRelease framework. The reconstructed MC events contains reconstructed vertex and tracks informations. Before comparison Data and MC events, the

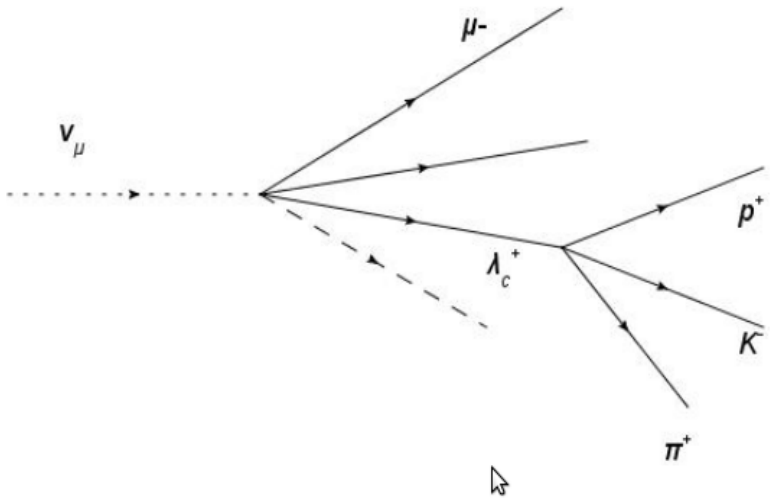

Figure 5.3: ν_μCC interaction with more than one vertex.

primary vertex in MC events must be defined since the mean number of reconstructed vertex is 2.2.

5.1 ν_μCC Events

After the event location and decay search, a file containing the information about the analyzed event is uploaded in the central Database at Lyon. This is called summary file which contains the vertex and track informations.

Based on the summary file, we have classified the Data as 2008-2009 and 2010 samples. Since the selection criteria for ν_μCC events was modified, for 2010 event analysis, a cut on muon momentum, P <15 GeV, is applied in order to improve the tau detection efficiency. The Data is further divided into two as events analyzed in Japan and in Europe in order to check possible biases in the event location.

In MC ν_μCC events, primary vertex tagging is rather simple if the muon track is reconstructed. The vertex with a muon track is defined as primary vertex. If muon track is not reconstructed in the event, the most upstream vertex is taken as a primary vertex. We have skipped location simulation assuming that location efficiency is flat for ν_μCC and ν_μCC-Charm events.

The Figure 5.4 show the multiplicity distribution for 2008-2009 Data sample. There is a

discrepancy between Data and MC events. In particular in the first bin, the discrepancy is very large. On the other hand, Japan sample shows a very good agreement with MC events. The comparison of charged particle slopes are given in Figures 5.5 and 5.6. In Europe sample, the agreement between Data and MC is satisfactory. But there is very small discrepancy at small angles. In the case of Japan sample, the agreement is satisfactory but similar to European case there is a small discrepancy in slope X but slope Y shows very good agreement between Data and MC.

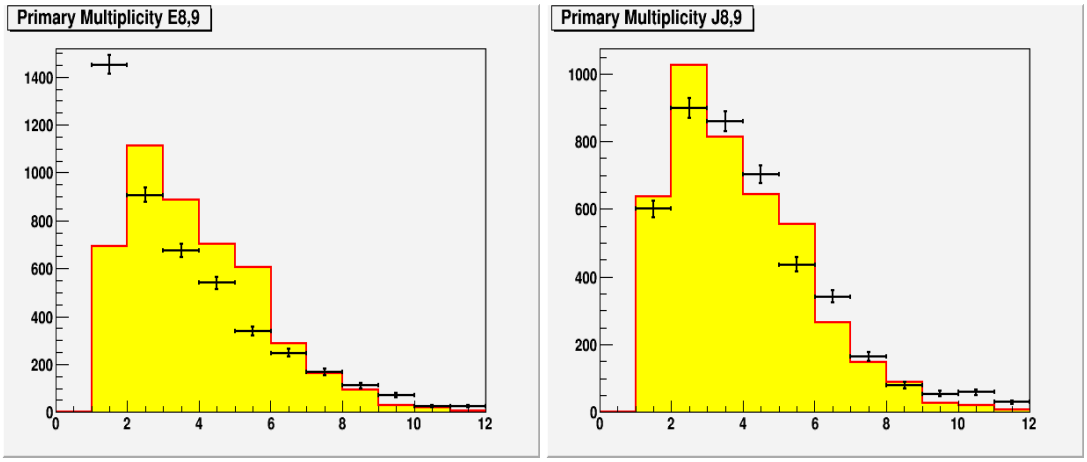

Figure 5.4: Primary multiplicity for 2008-2009; Left: European sample, Right: Japan sample.

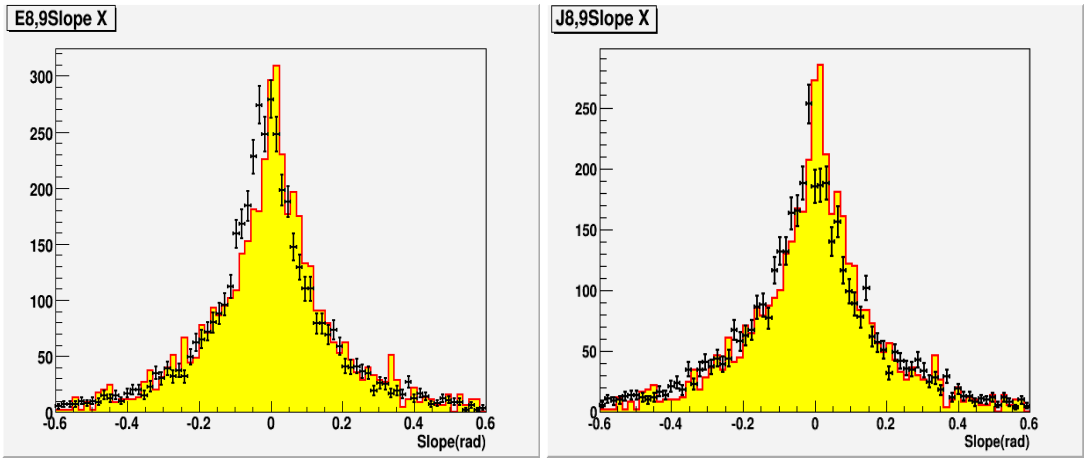

Figure 5.5: Charged slope X for 2008-2009; Left: European sample, Right: Japan sample.

Furthermore, the comparisons of 2010 Data sample are given in Figures 5.7, 5.8, and 5.9. In 2010 data sample the discrepancy in multiplicity distribution is striking for European sample. In the first bin of the distribution, that is events with a single multiplicity is much more in Data. However, the situation is opposite in the case of Japan sample. It means Data is less

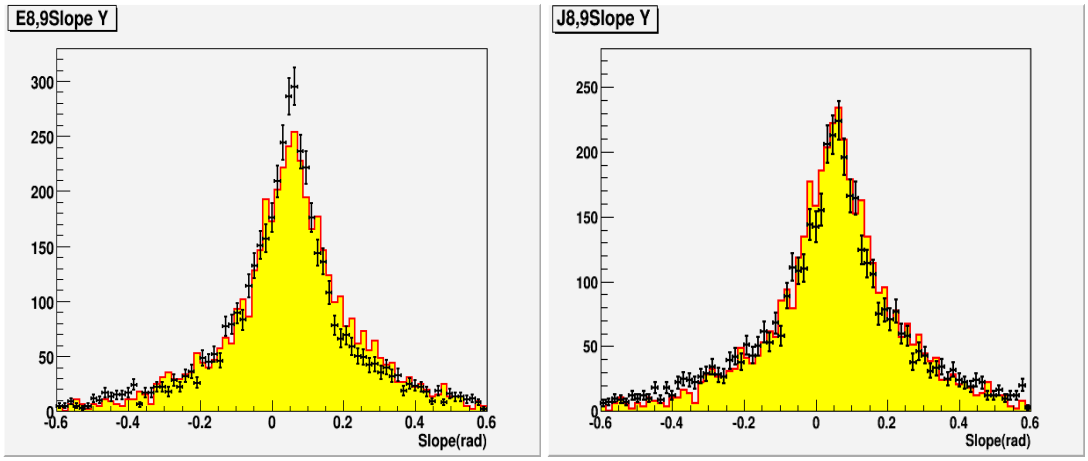

Figure 5.6: Charged slope Y for 2008-2009; Left: European sample, Right: Japan sample.

than MC in the first bin. Moreover, some discrepancies are also seen in slope distributions in particular for European sample. The Japan 2010 Data shows a good agreement with MC events.

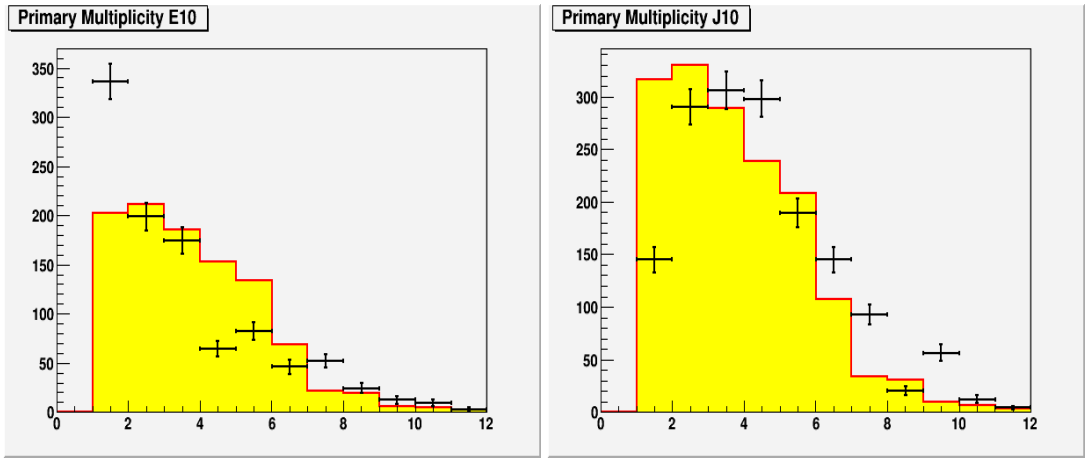

Figure 5.7: Primary multiplicity for 2010; Left: European sample, Right: Japan sample.

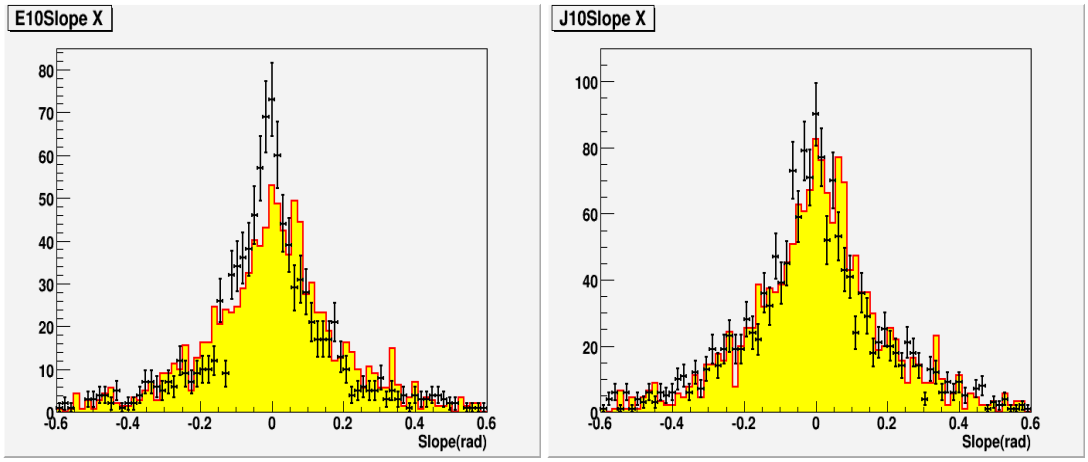

Figure 5.8: Charged slope X for 2010; Left: European sample, Right: Japan sample.

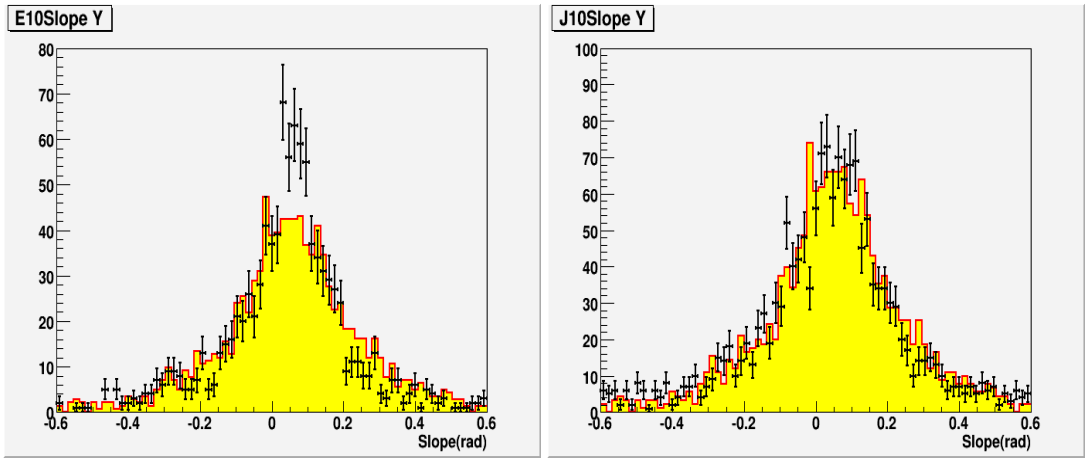

Figure 5.9: Charged slope Y for 2010; Left: European sample, Right: Japan sample.

The vertex position distributions for all events are given in Figures 5.10, 5.11, and 5.12. In general, MC reproduces Data well concerning the vertex positions.

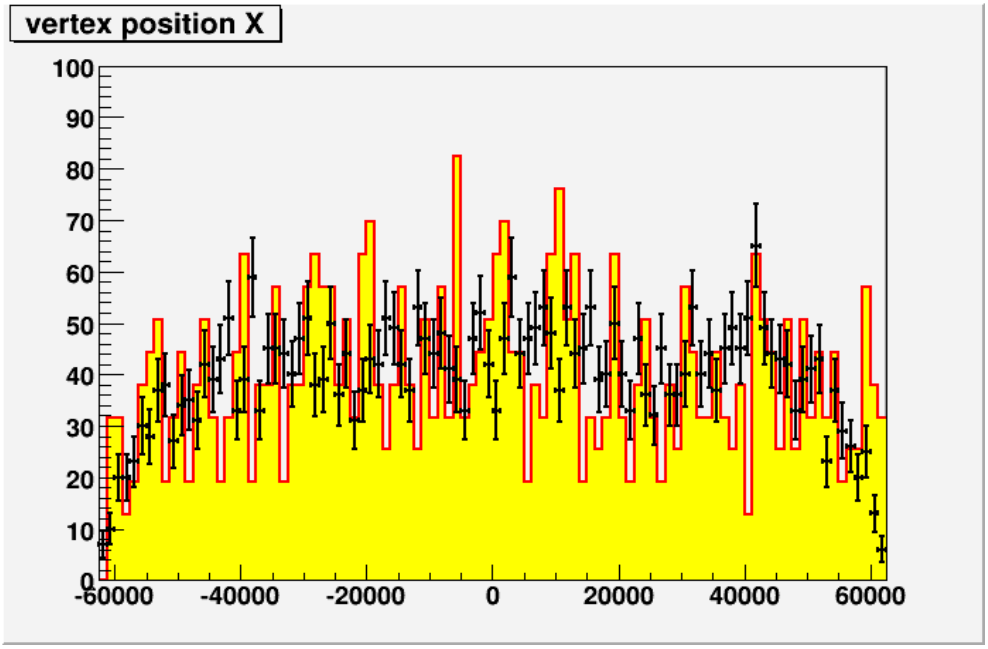

Figure 5.10: Vertex position of X for all events.

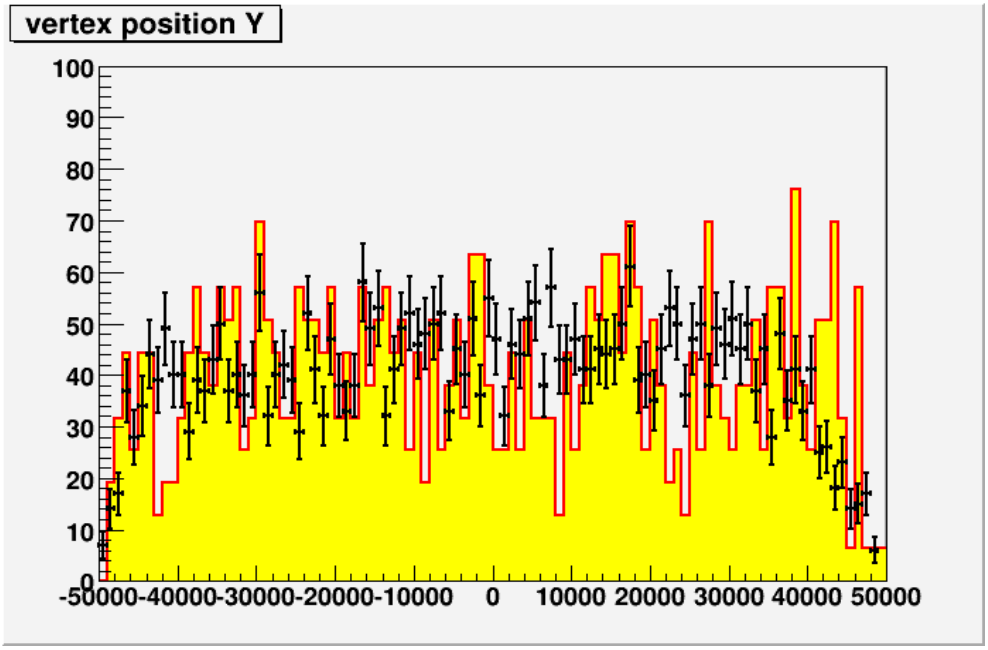

Figure 5.11: Vertex position of Y for all events.

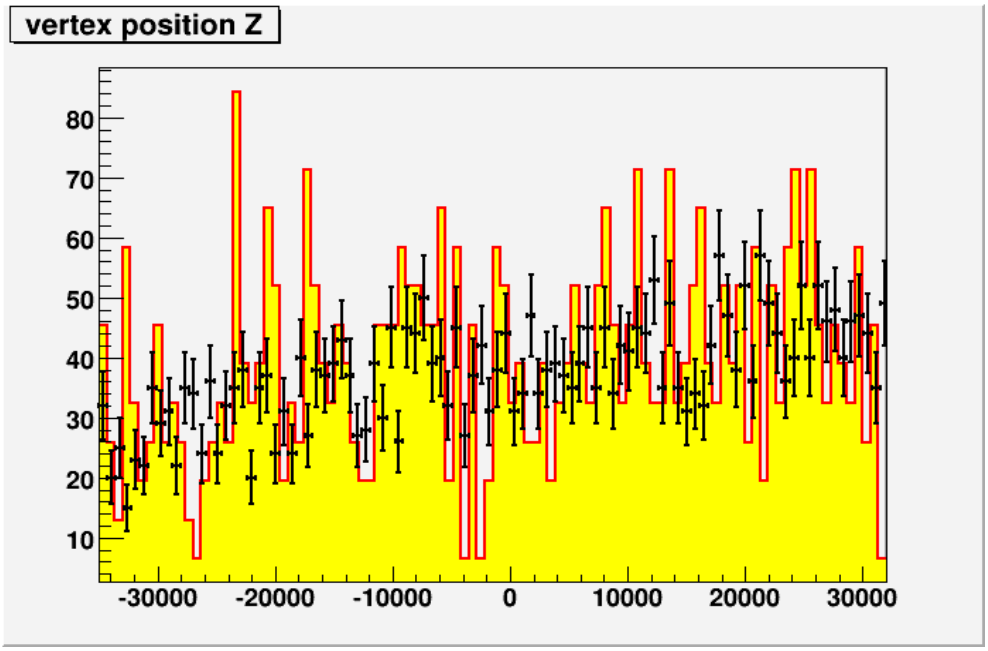

Figure 5.12: Vertex position of Z for all events.

5.2 ν_μCC-Charm Events

The study of charm events is particularly important for the oscillation analysis because these events constitute a background for ν_τ search. The flight length and decay topologies of charged charm and tau-lepton are very similar. In case if the primary lepton is not identified, the charmed-hadron is background for the oscillation signal. Furthermore, by studying the charm events we can demonstrate reliability of tau detection efficiency. Table 5.1 shows list of charm events and their decay topologies found in 2008-2009 and 2010 samples.

Table 5.1: Summary table of all charm events observed in 2008, 2009, and 2010.

Brick-ID	**Event-ID**	**Year**	**Topology**
34730	180718369	2007	kink
48057	233225467	2008	kink
85405	234654975	2008	4-Vee
44354	234276347	2008	kink
65097	222007691	2008	Vee
27222	234341013	2008	C2
72853	231012915	2008	S Vee
14653	228197639	2008	S Vee
79117	228563573	2008	S Vee
140875	233478285	2008	S Vee
127653	222274169	2008	trident
14714	236177101	2008	N1
66404	9214106181	2009	kink
59278	9317000655	2009	S trident
73646	9248074251	2009	Vee
150444	9153055713	2009	kink
35135	9231046733	2009	trident
48601	9306092701	2009	Vee
42759	9180028411	2009	Vee

Continued on next page

Table 5.1 – *Continued from previous page*

Brick-ID	**Event-ID**	**Year**	**Topology**
137454	9184112367	2009	Vee
118858	9189079481	2009	Vee
137009	9262083703	2009	N1
110205	9152034063	2009	S1
117643	9315114545	2009	S1
113324	9291027303	2009	S4
15574	927302960	2009	Vee
22777	10146003231	2010	Vee
33848	10207022839	2010	Vee
142664	10134047875	2010	kink
147363	225107648	2008	kink
51248	234539244	2008	kink
81191	23311658	2008	S1
33398	231062848	2008	N1
88427	233235784	2008	Vee
133606	224984190	2008	Vee
139294	237491736	2008	Vee
149995	237040910	2008	S1
15459	237403844	2008	S Vee
88951	230694744	2008	S trident
114409	230467340	2008	S1
134350	234231460	2008	S1
70300	9163097136	2009	Vee
131501	9175042230	2009	kink
37084	9253108902	2009	trident
22331	9185049172	2009	Vee
37626	9312041426	2009	kink
101750	9150262214	2009	Vee
83852	9302097642	2009	4Vee

Continued on next page

Table 5.1 – *Continued from previous page*

Brick-ID	Event-ID	Year	Topology
6502	9236112084	2009	S1
72495	9187032220	2009	S1
126388	9318073896	2009	S1

Given the limited statistics, the comparison of Data and MC is not conclusive. Figures 5.14 and 5.15 show the charmed slopes in X and Y. They show a reasonable agreement. Figures 5.16 and 5.17, shows flight length distribution of charmed hadron and Φ-angle distribution. There are some discrepancies, in particular Φ-angle distribution.

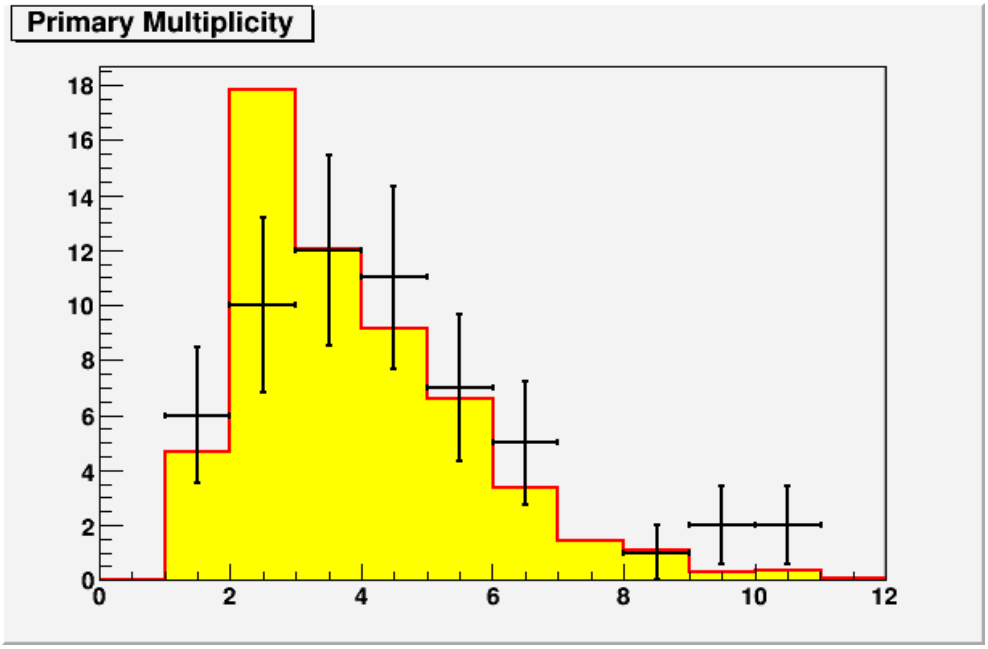

Figure 5.13: Primary multiplicity for charm particles.

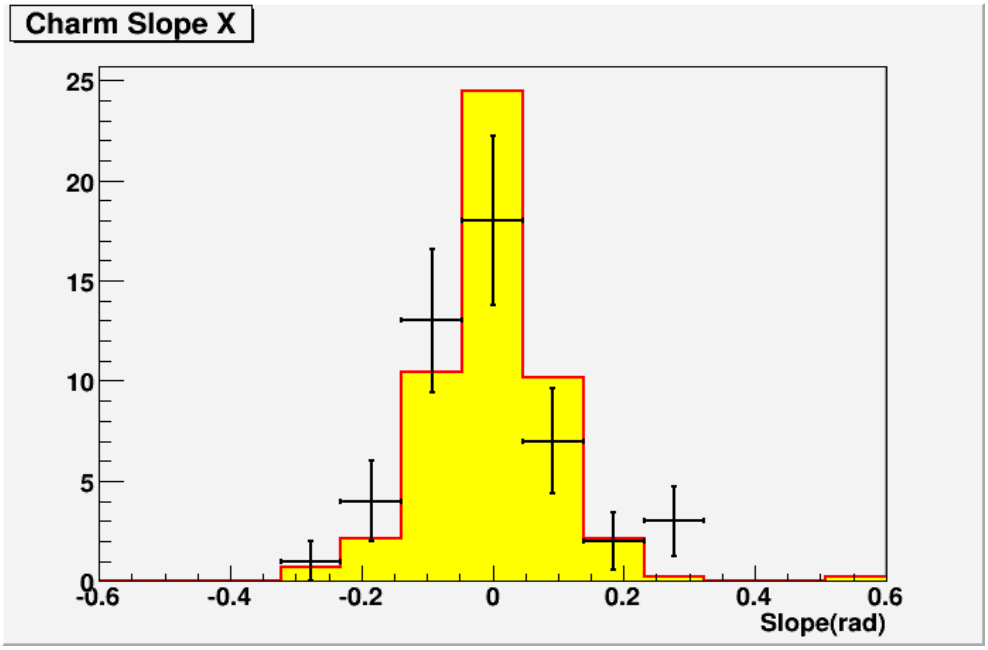

Figure 5.14: Charm Slope of X.

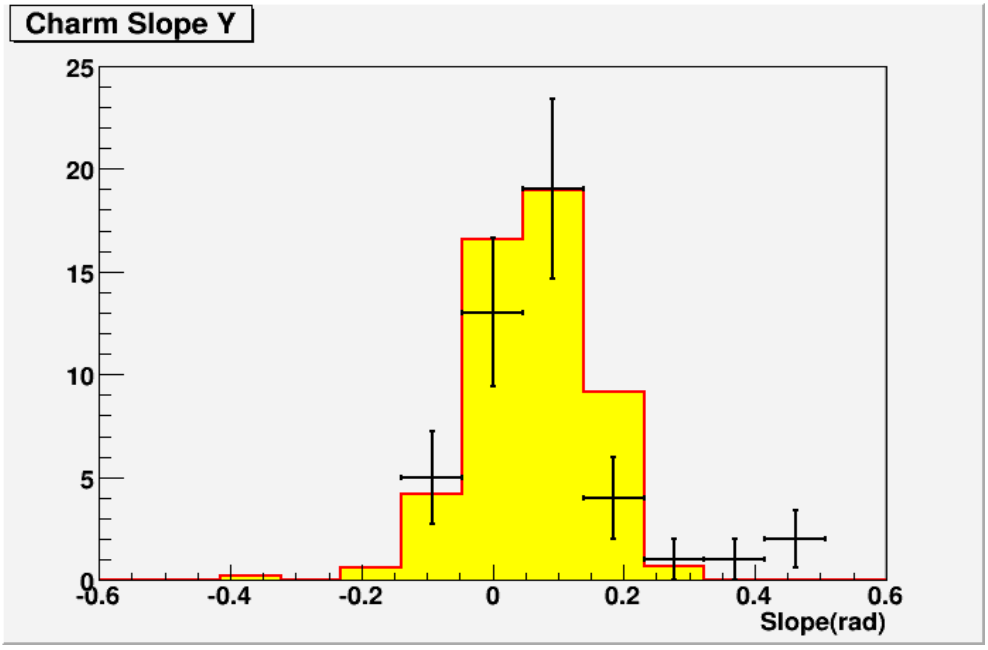

Figure 5.15: Charm Slope of Y.

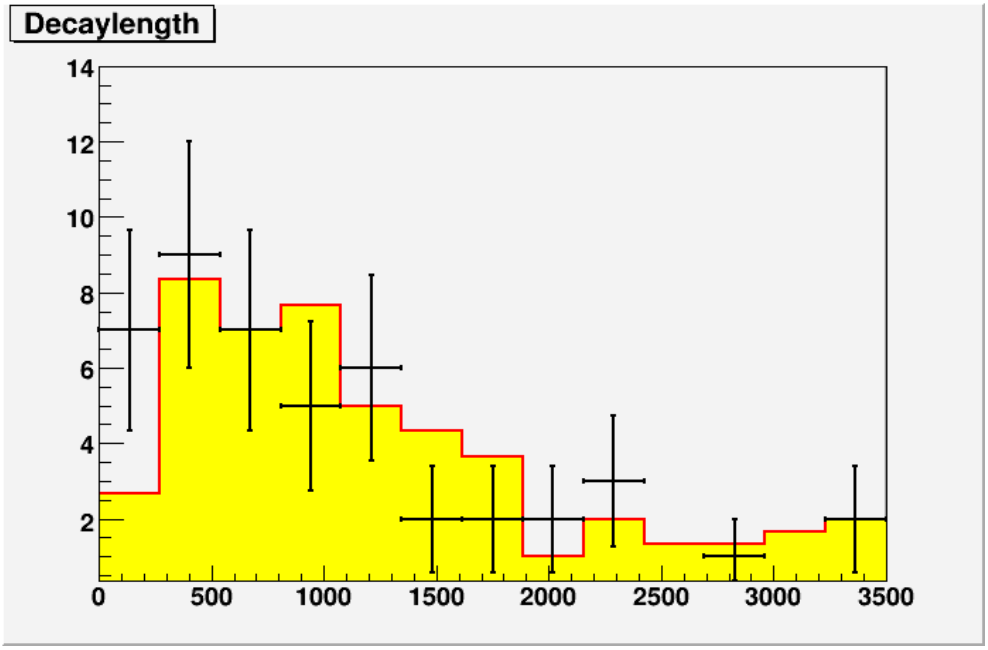

Figure 5.16: The decay length of charm particles.

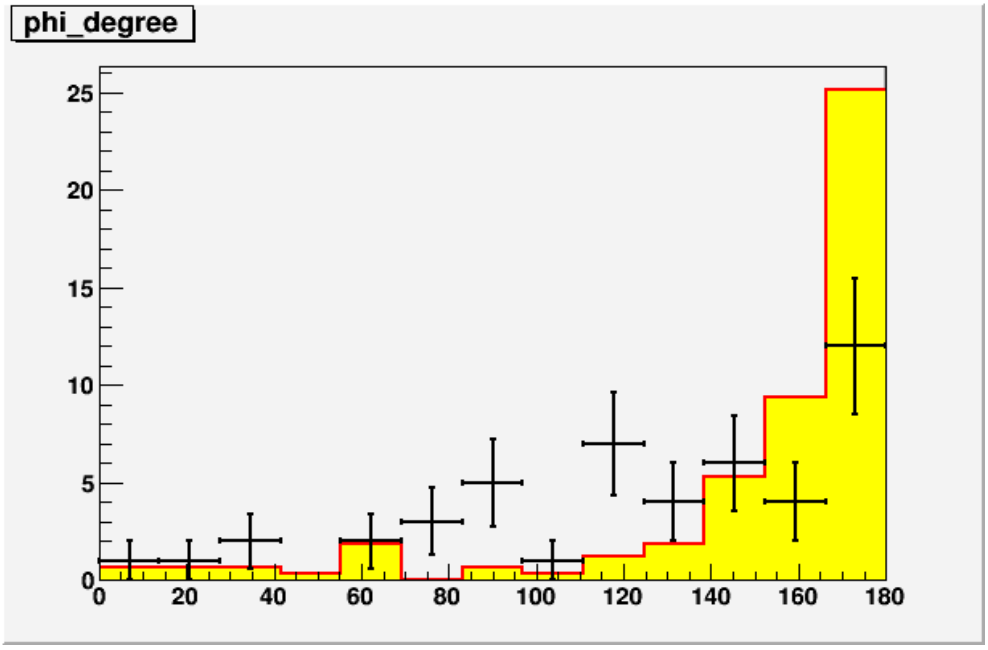

Figure 5.17: Φ angle for charm particles.

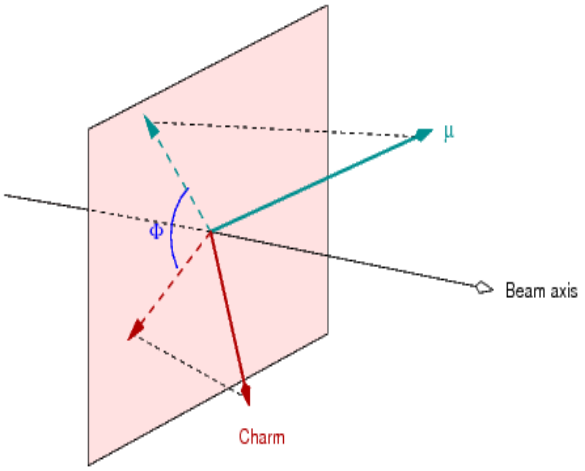

Figure 5.18: Definition of angle Φ.

Figures 5.19,5.20 and 5.21 show the vertex position distribution. Although X and Y positions give a reasonable agreement, in Z position there is discrepancy that should be understood. In data there are events out of the brick. This may be due to a typing error during feedback file preparation.

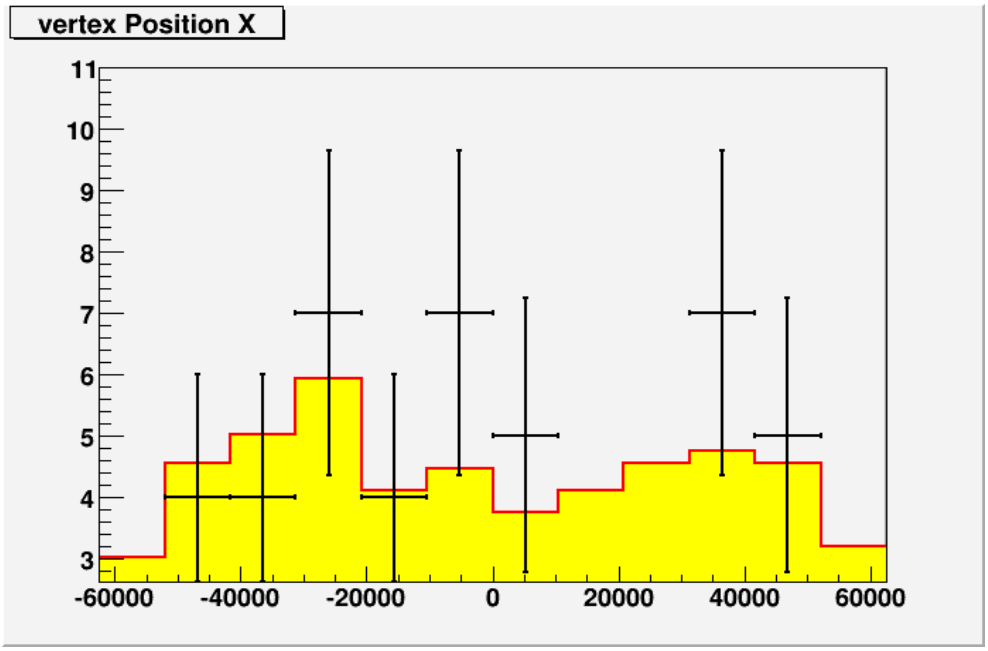

Figure 5.19: Vertex position of X for charm particles.

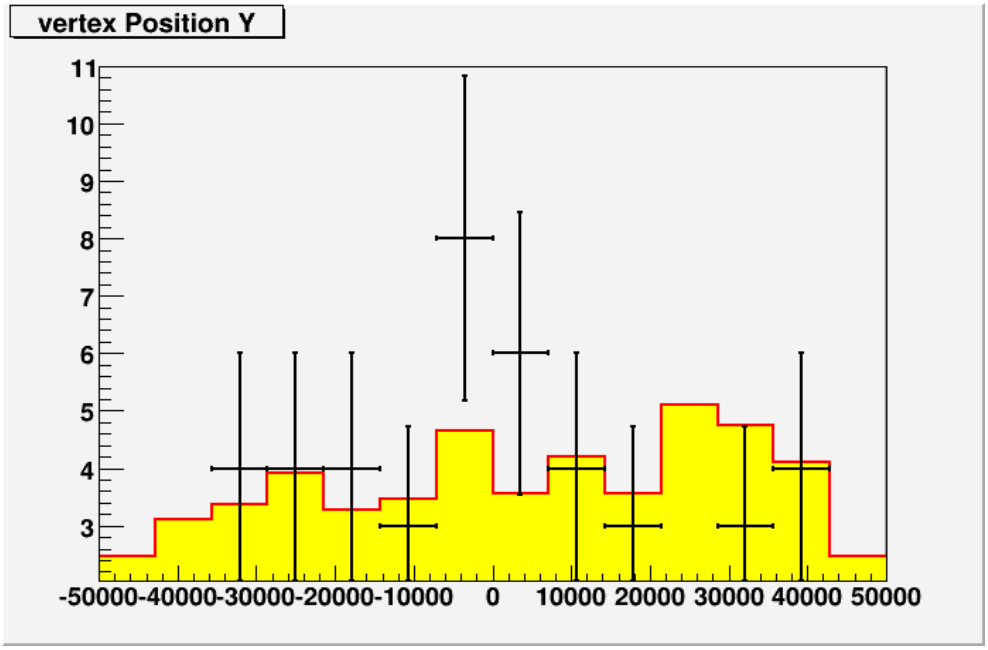

Figure 5.20: Vertex position of Y for charm particles.

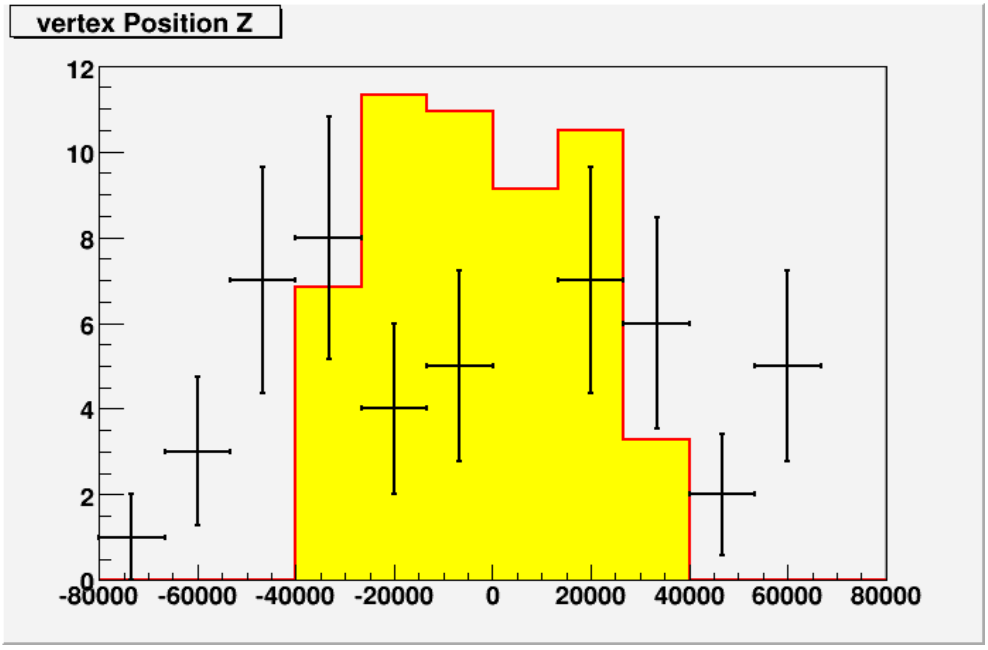

Figure 5.21: Vertex position of Z for charm particles.

CHAPTER 6

CONCLUSIONS

As a long-base line experiment, OPERA aims to prove $\nu_\mu \rightarrow \nu_\tau$ oscillation through direct observation of ν_τ Charged Current interactions in the ECC brick. The OPERA detector is located in Gran Sasso underground laboratory, 732 km away from CERN where CNGS neutrino beam is produced. The data taking was started in 2007 and is going on smootly. So far, about 4000 neutrino interactions have been analyzed and two ν_τ CC interactions have been identified.

In September 2011, An automatic emulsion microscope was installed in emulsion scanning laboratory at Middle East Technical University (METU). After basic tests and fine tunings the system is fully operative since the the beginning of 2012. In this thesis we have given the scanning and analysis results of the events located with Ankara Microscope.

Moreover, a detailed Data/Monte Carlo (MC) comparisons of ν_μCC and ν_μCC-Charm events have been done. For this comparison Data is classified according to run year as 2008-2009 and 2010 samples. Further classification has been done based on scanning labs as European and Japan. In general, the agreement between Data and MC is satisfactory. But in multiplicity distribution it seems that in European sample there are more events with a single multiplicity then MC expectation. This could be due to low efficiency for the large angle tracks. The discrepancies in 2010 Data could be due to fact that only a small fraction of 2010 events are analyzed. The biased in event location could be removed when the analysis of full sample of 2010 events is completed. Concerning the charm sample, there is a reasonable agreement between Data and MC. Since sample size is limited to 51 events, the comparisons are not so conclusive. This analysis should be repeated including the scanning simulations for the event location procedure.

REFERENCES

[1] Robert G. Arns, *Detecting the Neutrino*, Phys.pers. 3 314-334, 2001.

[2] M. Riordan, *Pauli's Ghost: The Conception and Discovery of Neutrinos*, in Current Aspects of Neutrino Physics ed. by D.O. Caldwell (Springer-Verlag Berlin Heidelberg New York), 2001.

[3] B. Kayser and R.N. Mohapatra, *The Nature of Massive Neutrinos*, in Current Aspects of Neutrino Physics ed. by D.O. Caldwell (Springer - Verlag Berlin Heidelberg New York), 2001.

[4] F. Reines, *The Neutrino: From Poltergeistto Particle*, University of California, 1995.

[5] R. Davis Jr., Phys.Rev.Lett. 12, 303-305, 1964.

[6] LAPP web page, http://lappweb.in2p3.fr/neutrinos/anhistory.html. Retrieved on May 01, 2012.

[7] CERN web page, http://public.web.cern.ch/public/en/about/Nobels-en.html. Retrieved on May 05, 2012.

[8] SLAC web page, www.slac.stanford.edu/. Retrieved on May 05, 2012.

[9] DONUT Collaboration K. Kodama et al., Phys.Lett. B504:218-224, 2001.

[10] W. N. Cottingham and D. A. Greenwood, *The Nature of Massive Neutrinos*, An Introduction to the Standard Model of Particle Physics, 2007.

[11] J. Bonn et al., Prog.Part.Nucl.Phys. 48, 133, 2002; V. M. Lobashev et al., Nucl.Phys.Proc.Suppl. 91, 280, 2001.

[12] K. Assamagan et al., Preprint No. PSI-PR-94-19, 1994.

[13] D. Buskulic et al., Phys. Lett. B349, 585, 1995.

[14] H. Back et al., hep-ex/0412016v2, 2005.

[15] Z. Maki, M. Nakagawa, and S. Sakata. Remarks on the Unified Model of Elementary Particles. Progress of Theoretical Physics, 28:870-880, 1962.

[16] L. Consiglio, *Algorithms for the analysis of neutrino interactions in the OPERA-like Emulsion Cloud Chambers*, (Doctoral dissertation), University of Bologna, 2007.

[17] ATNF web page, http://outreach.atnf.csiro.au/education/senior/astrophysics/stellarevolution-mainsequence.html. Retrieved on May 01, 2012.

[18] G.L. Fogli, E. Lisi, *Standard solar model uncertainties and their correlations in theanalysis of the solar neutrino problem*, DOI:10.1016/0927-6505, 1994.

[19] H. Klapdor-Kleingrothaus et al., Particle Astrophysics, DOI: 10.1201/9781420050462, 1999.

[20] The GALLEX Collaboration, P. Anselmann et al:, Phys. Lett. B285 376, 1992.

[21] J. N. Abdurashitov et al:, J. Exp. Theor. Phys. 95 181, 2002.

[22] S. M. Kireev, published in Neorganicheskie Materialy, Vol. 47, No. 12, pp. 1413-1421, 2011.

[23] A. Murat Guler, *D^0 production rate measurement in neutrino interactions and a limit on muon neutrinoto tau neutrino oscillation*, (Doctoral dissertation), Middle East Technical University, 2000.

[24] L. A. Whitehead, *Measurement of the Single Charged Pion Production Cross Section in Charged-Current Neutrino-Carbon Interactions*, (Doctoral dissertation), Stony Brook University, 2007.

[25] F. Pupilli, *Search for ν_τ interactions in the OPERA experiment*, (Doctoral dissertation), UNIVERSITA DEGLI STUDI DELLAQUILA, 2011.

[26] The SNO Collaboration, J. Boger et al., Nucl.Inst.Meth. A 449 172-207, 2000.

[27] K2K collaboration, Phys. Rev. Lett. 90 041801 (hep-ex/0212007), 2003; K2K collaboration, Phys. Rev. Lett. 94 081802 (hep-ex/0411038), 2005.

[28] MINOS Collaboration, arXiv: hep-ex/0605058 v2, 2006.

[29] T. M. Raufer, *A Study of Neutrino Oscillations in MINOS*, (Doctoral dissertation), University College, Oxford, 2007.

[30] The OPERA Collaboration, M. Guler et al., *An appearance experiment to search for $\nu_\mu \rightarrow \nu_\tau$ oscillations in the CNGS beam*, CERN/SPSC 028, 2000.

[31] M. De Serio, arXiv: s0910.0337v1, 2009.

[32] T. Strauss, *Charm production in the OPERA experiment and the study of a high temperature superconducting solenoid for a liquid argon time projection chamber*, (Doctoral dissertation), Humboldt Universitat zu Berlin, 2010.

[33] C. Bozza et al., Published in Nucl.Inst.Meth. A525:485-495, 2004.

[34] Yu. A. Gornushkin, *SEARCH FOR $\nu_\mu \rightarrow \nu_\tau$ OSCILLATIONS IN APPEARANCE MODE IN THE OPERA EXPERIMENT*, PACS: 14.60.Pq, 2011.

[35] CNGS Commissioning Team, K. Cornelis et al., *CERN Neutrinos to Gran Sasso (CNGS): Results from Commissioning* ,CERN-AB-039, 2007.

[36] CERN web page, http://projcngs.web.cern.ch/proj-cngs/. Retrieved on April 26, 2012.

[37] Parth Devshankar Upadhyay web page, http://parthdu.wordpress.com/. Retrieved on April 26, 2012.

[38] OPERA web page, http://www-opera.desy.de/detector.html. Retrieved on April 26, 2012.

[39] M. Guler et al., *The OPERA experiment in the CERN to Gran Sasso neutrino beam*, JINST 4 P04018, DOI:10.1088/1748-0221/4/04/P04018, 2009.

[40] A. Cazes, *Experience From OPERA*, PoS(Nufact08).048, 2008.

[41] N. Naganawa, *Emulsion Analysis in the OPERA Experiment*, Presentation at TAUP, 2009.

[42] CERN Courier web page, http://cerncourier.com/cws/article/cern/29754. Retrieved on April 26, 2012.

[43] INFN web page, http://web.na.infn.it/index.php?id=417. Retrieved on April 26, 2012.

[44] C. Jollet, *The OPERA experiment*, IReS, IN2P3-CNRS and University Louis Pasteur, 2006.

[45] A. Cazes, S. Dusini and Y. Gornushkin, *Electronic Detectors*, Poster session presented at NU2010, 2010.

[46] S. Dusini et al., Nucl.Inst.Meth. A508:175-180, 2003.

[47] D. Di Ferdinando, *Experimental study of neutrino interactions in the OPERA – like Emulsion Cloud Chambers*, (Doctoral dissertation), University of Bologna, 2007.

[48] A. Bergnoli et al., Nucl.Inst.Meth. A602:653-657, 2009.

[49] M. Guler et al., New J.Phys. 14 033017, 2012.

[50] N. Di Marco, *First results from the OPERA experiment*, Presentation, 2009.

[51] M. Cozzi, *Study of the pion identification in the Emulsion Cloud Chambers of the OPERA experiment*, (Doctoral dissertation), University of Bologna, 2005.

[52] S. Aoki, et al., Nucl.Inst.Meth. B51 466, 1990.

[53] N. D′Ambrosio, Nucl. Inst. Meth. A477 431, 2002; N. D′Ambrosi, Nucl. Inst. and Meth. A525 193, 2004; G. Sirri, *Automatic scanning of emulsion films for the OPERA experiment*, (Doctoral dissertation), University of Bologna, 2003.

[54] G. Sirri, *Automatic scanning of emulsion films for the OPERA experiment*, (Doctoral dissertation), University of Bologna, 2003.

[55] ROOT-CERN web page, http://root.cern.ch. Retrieved on May 5, 2012.

[56] S. Tufanli. *D^0 background to neutrino oscillations in the OPERA Experiment*. Master thesis, Middle East Technical University, 2009.

[57] S. Dusini. How to access data but also MC in OpEmuRec. OPERA Workshop, 2010.

[58] V. Tioukov, I. Kreslo, Y. Petukhov, and G. Sirri, Nucl.Inst.Meth. A559:103-105, 2006.

[59] C. Bozza et al. *SySal*: *System of Salerno*. arXiv:hep-ex/9901031, 1999.